



CD2⁺ T-helper 17-like cells differentiated from a CD133⁺ subpopulation of non-small cell lung carcinoma cells promote the growth of lung carcinoma

Miaomiao Jia^{1,2#}, Xianxian Jia^{1,2#}, Dong Zhang¹, Wenxuan Liu¹, Shanyong Yi³, Zhenhua Li⁴, Bin Cong^{1,2,3}, Chunling Ma^{2,3}, Shujin Li^{2,3}, Jun Zhang¹

¹Institute of Basic Medicine, Hebei Medical University, Shijiazhuang, China; ²Research Unit of Digestive Tract Microecosystem Pharmacology and Toxicology, Chinese Academy of Medical Sciences, Shijiazhuang, China; ³College of Forensic Medicine, Hebei Key Laboratory of Forensic Medicine, Collaborative Innovation Center of Forensic Medical Molecular Identification, Hebei Medical University, Shijiazhuang, China; ⁴Department of Thoracic Surgery, The Fourth Hospital of Hebei Medical University, Shijiazhuang, China

Contributions: (I) Conception and design: B Cong; (II) Administrative support: C Ma, S Li; (III) Provision of study materials or patients: Z Li, S Yi; (IV) Collection and assembly of data: M Jia; (V) Data analysis and interpretation: X Jia; (VI) Manuscript writing: All authors; (VII) Final approval of manuscript: All authors.

[#]These authors equally contributed to this work.

Correspondence to: Bin Cong. Institute of basic Medicine, Hebei Medical University, No. 361 Zhongshan East Road, Shijiazhuang 050017, China. Email: hbydbincong@126.com.

Background: Cancer stem cells (CSCs) give rise to a diverse variety of differentiated cells, which comprise the bulk of the tumor microenvironment (TME). However, the exact multi-directional differentiation potential of CSCs has not been fully clarified. This study was designed to explore whether CSCs differentiate into cellular components of the TME to promote the growth of lung carcinoma.

Methods: The present of CD133⁺, CD2⁺, and CD133⁺CD2⁺ cells in both clinical lung adenocarcinoma tissue and non-small cell lung carcinoma (NSCLC) cell lines were monitored using polymerase chain reaction (PCR) Array, flow cytometry (FCM), quantitative real-time PCR (qRT-PCR) and immunohistochemistry (IF). Stem-like properties of CD133⁺ cells and CD2⁺ cells were detected by sphere formation assay, IF, and western blot. Colony formation and xenograft tumors experiments were performed to assess the malignant behaviors of CD2⁺ cells. The differentiation of CD133⁺ cells to CD2⁺ Th17-like cells was observed by FCM. The interleukin (IL)-2/phosphorylated signal transducer and activator of transcription protein 5 (pSTAT5)/retinoic acid receptor-related orphan receptor gamma t (RORγt) signaling pathway was evaluated by western blot and FCM.

Results: We found that CD133⁺ cells within both clinical lung adenocarcinoma tissue and NSCLC cell lines included a subset of CD2-expressing cells, which were correlated with the grade of malignancy ($r=0.7835$, $P<0.01$) and exhibited stem-like properties. Then, we determined the tumorigenic effects of CD2 on the growth of transplanted Lewis lung carcinoma cells (LLC1) in C57/BL6 mice. The results indicated that CD2⁺ cells were effective in promoting tumor growth *in vivo* ($P<0.01$). Furthermore, we obtained direct evidence of an ability of CD133⁺ cells to transform to T-helper 17-like cells via an intermediate CD133⁺CD2⁺ progenitor cell that is able to secrete IL-17A and IL-23. Furthermore, we found that IL-2 can inhibit the production of T-helper 17-like cells ($P<0.001$) by modulating the activation of STAT5 signaling pathways to downregulate the expression of RORγt ($P<0.001$).

Conclusions: Our data demonstrates that Th17-like cells generated from CSCs support cancer progression. These findings enrich the definition of multidirectional differentiation potential of CSCs and improve the understanding of the role of CSCs in cancer progression, which aids the improvement and creation of therapies.

Keywords: Non-small cell lung carcinoma (NSCLC); cancer stem cells (CSCs); differentiation; tumor microenvironment (TME); Th17

Submitted Jan 20, 2021. Accepted for publication Apr 15, 2021.

doi: 10.21037/atm-21-980

View this article at: <http://dx.doi.org/10.21037/atm-21-980>

Introduction

Non-small cell lung carcinoma (NSCLC) is the most commonly diagnosed cancer and the leading cause of cancer-associated death (1). The prognosis of NSCLC is poor, and the survival rate is only 15% after 5 years because many of these patients ultimately do not respond to chemoradiotherapy, which is associated with unimaginable degree of cellular heterogeneity within a single tumor (2). The heterogeneity of tumor may correlates with cancer stem cells (CSCs) or tumor-initiating cells (TICs) which may be responsible for NSCLC treatment failure which includes local recurrence, distant metastasis, and the limitations of therapeutic agents (3). CSCs, which have been identified in most types of cancer, possess the capabilities of self-renewal, infinite proliferation, and multi-directional differentiation (4). Therefore, further efforts dedicated to uncovering the biological characteristics of these cells are urgently needed.

Tumor microenvironment (TME) is the cellular environment in which the CSCs exists (5). In addition to CSCs, the TME is composed of immune cells, blood vessels, fibroblasts, smooth muscle cells, some epithelial cells, and extracellular matrix (6). CSCs maintain intricate interactions with other malignant cells within the TME largely influencing the outcome of cancer growth and metastasis. They have been certified that TME related features, especially immune and stromal cell promote the development of diagnostic and prognostic assessment process of NSCLC (7). Moreover, the metabolic state and activities of the immune cells comprising the TME influences the proliferative and invasive capacity of tumor cells.

The immune cells in the TME are related to poor elimination of tumor cells, including a lack of strong cancer antigens or epitopes recognized by T cells, minimal activation of cancer-specific T cells, poor infiltration of T cells into tumors, downregulation of the major histocompatibility complex on cancer cells, as well as immunosuppressive factors and cells in the TME (8). In addition to cytokines and infiltrating immune cells, other cells in the TME also suppress the immune system (9).

These cells may act as intermediaries, triggering a cascade of events that ultimately culminates in immunosuppression; however, the actual causes remain poorly defined.

It has been shown that a positive response of the body in eliminating tumor cells usually depends on the interaction of tumor cells with immune cells in the TME (10). When these interactions occur, the relationship between tumor cells and immune cells in the TME plays an important role in inhibiting or enhancing the immune response (11). The occurrence, development, and outcome of the tumor depends on the function of the immune cells in the TME and is determined by T-cell immunity (8). T cells provide signals for the identification and killing of cancer cells. These signals are essential to the protective immune response against tumors. The CSCs in the CSC niche, as well as in the TME, add complexity to tumor immunity (12,13). Owing to this complexity, further investigation is required to uncover the relationship between CSCs and T cells in the TME.

Recent studies on CSCs have shown that glioblastoma stem-like cells and colorectal CSCs are multipotent and have differentiation potential along tumor and endothelial lineages (14,15). Also, murine mammary gland tumor cells demonstrating CSC characteristics can become functional adipocytes (16), and neurons generated from CSCs support cancer progression (17). These observations indicate that the cells in the TME could enter through infiltration or result from CSC differentiation. Consistent with this hypothesis, the presence of some immune cells within tumors is ascribable to infiltration and trafficking, whereas others may actually originate from the tumor itself. The biomarkers and effects on the tumorigenesis and development of these immune cells with different origin need to be further clarified.

This study was designed to test the potential of CSCs to differentiate into neoplastic immune cells and evaluate the capacity of immune-like cells to participate in the process of tumorigenesis. The significance of neoplastic immune cells to the prognosis of NSCLC patients was also analyzed.

We present the following article in accordance with the ARRIVE reporting checklist (available at <http://dx.doi.org/10.21037/atm-21-980>)

org/10.21037/atm-21-980).

Methods

Cell culture and reagents

Human non-small cell lung cancer A549 cells and Lewis lung carcinoma cells (LLC1) obtained from the Shanghai Institutes for Biological Sciences were validated by short tandem repeat (STR) DNA profiling and tested for mycoplasma. Cells were cultured in Roswell Park Memorial Institute (RPMI) 1640 or Dulbecco's Modified Eagle Medium (DMEM) (Invitrogen) supplemented with 10% fetal bovine serum (FBS, Gibco) and 1X penicillin/streptomycin (Gibco) at 37 °C in 5% CO₂.

Cell isolation and culture

CD133⁺ cells were isolated by magnetic-activated cell sorting (MACS) with a CD133 MicroBead Tumor Tissue Kit (Miltenyi Biotec, 130-100-857) using methods described previously (18). The cells were cultured in serum-free media for sphere formation assays. When we explored whether the cytokines had a role in the differentiation, 10 ng/mL of interleukin (IL)-2, IL-3, IL-6, or transforming growth factor beta (TGF-β) was added to the culture for 24 hours. CD133⁺ cells from clinical tumor specimens were isolated by flow cytometry (FCM). CD2⁺ and CD2⁻ cells were isolated by MACS with CD2 MicroBeads (Miltenyi Biotec, 130-091-114).

FCM

A single cell suspension was obtained by grinding and filtering tissue, and the A549 cell suspension was digested with trypsin. All cells were resuspended in wash buffer (PBS containing 0.1% BSA) and stained for surface markers using FITC Mouse Anti-Human CD2 (BD Biosciences, 555326), FITC Mouse Anti-Human CD4 (BD Biosciences, 550628), FITC Mouse IgG1, κ Isotype Control (BD Biosciences, 555748), CD133/1 Antibody, anti-human, APC (Miltenyi Biotec, 130-113-668), and isotype control antibodies, mouse IgG1, APC (Miltenyi Biotec, 130-113-196). FCM data were acquired with a FACSCalibur (BD Biosciences). All used antibodies were list in [Table S1](#).

Cell immunofluorescence staining

Immunofluorescence staining was performed as described

previously (18). Briefly, primary antibodies were added to cells and incubated for approximately 90 minutes at 4 °C. Nuclei were stained with 4'-6-diamidino-2-phenylindole (DAPI). All immunofluorescence staining results of *in vitro* cell culture were replicated more than 5 times. The primary antibodies used were FITC Mouse Anti-Human CD2 (BD Biosciences, 555326) and CD133/1 Antibody, anti-human, APC (Miltenyi Biotec, 130-113-668). All used antibodies were list in [Table S1](#).

Real-time quantitative polymerase chain reaction

The levels of messenger RNA (mRNA) expression were determined by quantitative polymerase chain reaction (qPCR) performed using an ABI PRISM 7500 Cycler (Applied Biosystems). Primers that resulted in amplification were designed from human structural genes and are listed in [Table S2](#). Following isolation of RNA from cell lines and its conversion to cDNA, qPCR quantitation was performed as described previously (18). RNA isolation and reverse transcription of CD133⁺ cells from human lung tissue specimens were performed using the REPLI-g WTA Single Cell Kit (QIAGEN,150063).

PCR array

Total RNA was obtained from cells using a RNeasy Mini Kit (QIAGEN, 74104). During RNA purification, an RNase-Free DNase Set (QIAGEN, 79254) was used for efficient on-column digestion of tiny amounts of DNA. RNA concentration quality control was performed using 1% agarose electrophoresis and the NanoQ Micro-volume Spectrophotometer (Capital Bio). Template cDNA was made using an RT2 First Strand Kit (QIAGEN, 330401). RNA isolation and reverse transcription of CD133⁺ cells from human lung tissue specimens were performed following the same steps as those described for real-time quantitative PCR.

Next, the cDNA was mixed with an appropriate amount of RT2 SYBR Green ROX qPCR Master mix (QIAGEN, 330522). The mixture was then aliquoted into wells of the Human Terminal Differentiation Markers RT² Profiler PCR Array (QIAGEN, 330231 PAHS-048ZA) or the Human Cell Surface Markers RT² Profiler PCR Array (QIAGEN, 330231 PAHS-055ZA). PCR was performed, and the relative gene expression was determined with data from a real-time cycler (Applied Biosystems 7500), using the $\Delta\Delta C_t$ method. All experiments were completed according

to the manufacturers' guidelines.

Enzyme-linked immunosorbent assay (ELISA)

After 12, 24, 36, and 48 hours of culture of isolated cells, supernatants were harvested. ELISAs were performed using the Human IL-17A ELISA kit (Invitrogen, KAC1591) and the Human IL-22 Sunny ELISA kit (Invitrogen, BMS2047). For each assay conducted, we followed the specific experimental steps set out in the manufacturers' instructions.

Western blot

Cells were collected and lysed in RIPA lysis buffer with added phenylmethylsulfonyl fluoride (PMSF). We detected the sample protein concentration using the BCA method (MULTI SCIENCES, BCA Protein Quantitation Kit, LK-PQ0012). Equal amounts of protein were separated using 10% sodium dodecyl sulfate-polyacrylamide gel electrophoresis (SDS-PAGE) and transferred to polyvinylidene difluoride membranes. The membranes were blocked using 5% nonfat milk and incubated overnight with the following primary antibodies: octamer-binding transcription factor-4 (Oct4) Antibody (Cell Signaling, 2750, 1:1,000), SRY-related high-mobility-group (HMG)-box protein-2 (Sox2) (D6D9) XP[®] Rabbit mAb (Cell Signaling, 3579, 1:1,000), Nanog (D73G4) XP[®] Rabbit mAb (Cell Signaling, 4903, 1:2,000), Signal transducer and activator of transcription protein 5 (Stat5) (D3N2B) Rabbit mAb (Cell Signaling, 25656, 1:1,000), Phospho-Stat5 (Tyr694) (D47E7) XP[®] Rabbit mAb (Cell Signaling, 4322, 1:1,000), retinoic acid receptor-related orphan receptor gamma t (ROR γ t) Monoclonal Antibody (Invitrogen, 14-6988-82, 1:800) and β -Actin (Cell Signaling, 4970, 1:1,000). After incubation, the membranes were washed and then incubated a second time with horseradish peroxidase-conjugated secondary antibodies. Finally, the blots on the membranes were visualized with enhanced chemiluminescence plus reagents (Life Technologies, Novex[®] Chemiluminescent Substrates, WP20005). All used antibodies were list in [Table S1](#).

Animal experiment

For the animal study, 4- to 6-week-old male C57/BL6 mice were purchased from Beijing Vital River Laboratory Animal Technology Co., Ltd. (Beijing, China). The mice

were housed in a conventional animal house under standard laboratory conditions, with a 12-hour light/12-hour dark cycle and a constant temperature (22 ± 1 °C) and humidity ($55\pm 5\%$). Standard rodent chow and tap water were freely available. All animal experiments were performed according to the Guidelines for the Care and Use of Laboratory Animals. The experimental protocols were approved by the Local Committee on Animal Care, Use and Protection of Hebei Medical University. The approval file for study related to animal experiment was No. 20190051. They were randomly assigned to 3 groups. After at least 5 days of acclimatization, the C57/BL6 mice were subcutaneously injected with 1×10^6 LLC1 cells in 100 μ L PBS via the right flank. In the experiments, each group comprised 5 mice. The size of each subcutaneously transplanted tumor was measured with the Vevo 2100 Imaging Platform (Visual Sonics, Canada). The tumor volume was calculated with the following formula: tumor volume = $0.5 \times \text{long diameter} \times \text{short diameter}^2$.

Human lung tissue specimen experiment

For the experiment, we used fresh lung cancer tissue samples that were collected between 2018 and 2020 from surgically resected specimens under approved research protocols. The pathological diagnoses were made by the pathology department of a local hospital according to the TNM staging system (tumor size, node involvement, metastasis presence). Stage I, II, and IIIA NSCLC samples were identified as adenocarcinoma by pathological histology. None of the patients had a direct blood relationship, or had received radiotherapy or chemotherapy preoperatively. Informed written consent was obtained from all the patients involved in the study. This study was approved by the Institutional Review Board of Hebei Medical University (No. 20190066) and conformed to the provisions of the Declaration of Helsinki (as revised in 2013). Hematoxylin and eosin (H&E) staining of the adenocarcinoma tissues was performed as described previously (19). Some sections were then stained for tissue immunofluorescence staining following the manufacturers' protocols. The primary antibodies used were Rabbit Anti-CD133 antibody (Abcam, ab19898), Mouse Anti-CD2 antibody (Abcam, ab193344), and Mouse Anti-CD4 antibody (Abcam, ab25804). The secondary antibodies were Alexa Fluor 488 Goat anti-Mouse IgG antibody (Invitrogen, A-21121) and Alexa Fluor 594 Goat anti-Rabbit IgG antibody (Invitrogen, R37117). All used

antibodies were listed in [Table S1](#).

Cell Counting Kit-8 (CCK-8) assay

The viability of cells after the indicated treatment was measured by CCK-8 assay (Dojindo, Japan) according to the manufacturer's instructions. Briefly, 5×10^3 cells/well were seeded into 96-well plates. When we explored whether the cytokines had a role in the survival of cells, 10 ng/mL of IL-2, IL-3, IL-6, or TGF- β was added to the culture for 24 hours. The absorbance of the converted dye was measured at 450 nm using a microplate reader (Thermo Fisher, Finland).

Colony formation assay

Cells were seeded into a 6-well plate and cultured for 10–14 days. Then, the colonies were fixed with 20% methanol and stained with 0.1% crystal violet dye. Representative images were obtained, and the colonies were counted.

Silencing of STAT5 by small interfering RNA (siRNA)

siRNA transfection was performed according to the manufacturer's instructions. Briefly, 4×10^5 A549/DDP cells were seeded into 6-well plates for 12 hours in the culture medium. Then, STAT5 siRNA (Cell Signaling Technology, 6275) and control siRNA (Cell Signaling Technology, 6275) were transfected with HiPerFect Transfection Reagent (QIAGEN, 301704). Following 48 hours of incubation, STAT5 expression was measured by western blot and qPCR.

Statistical analysis

Data were analyzed using GraphPad Prism (GraphPad 8.0). Unless otherwise noted, data were presented as the mean and standard deviation (SD). The number of experimental and control groups was at least 5. One-way analysis of variance (ANOVA) and unpaired *t*-tests were used as appropriate. Spearman's correlation tests were also performed. P values were considered significant at $P < 0.05$.

Results

CD133⁺CD2⁺ cells existed in NSCLC and were correlated with a poor prognosis

CD133 (also known as AC133 or prominin-1), a cell-surface glycoprotein, marks self-renewing cancer stem cells (CSCs)

in a variety of solid tumors, including those in the brain, colon, pancreas, prostate, liver, and lung (20). CD133⁺ CSCs are known markers of chemo- and radio-resistance in multiple aggressive cancers, that may drive intra-tumoral heterogeneity (21). In the present research, tumor tissues were collected from NSCLC patients undergoing surgery and analyzed by H&E staining. The results showed that the carcinoma samples showed significant characteristics of NSCLC. Cancer cells in lung adenocarcinoma tissues were irregularly arranged and cytological atypia was present (*Figure 1A*). Then, we performed a series analysis of the presence of CD133⁺ cells in NSCLC and para-carcinoma tissues using real-time PCR and FCM. It was confirmed that the CD133 expression levels of both mRNA (*Figure 1B*) and protein (*Figure 1C,D*) were significantly higher in tumor tissues than in adjacent non-tumor tissues. All of these results suggested the presence of CD133⁺ cells in NSCLC.

Next, we isolated CD133⁺ cells from human lung adenocarcinoma tissue by fluorescence-activated cell sorting (FACS) to study the phenotypes and characteristics of CD133⁺ cells. After sorting, the CD133⁺ cells were enriched to a purity of 97% (*Figure S1*). Then, the gene expression profiles of these cells were assessed using the Human Terminal Differentiation Markers RT² Profiler PCR Array. The result of the PCR array showed that CD133⁺ cells expressed specific genes in 13 tissues (*Figure S2A* and *Table S3*), including 7 bone marrow cell-related genes (*Figure 2A*). Bone marrow is known to be an important source of immune cells.

To confirm the specificity of the differentiation program, markers of other cell types were further examined using another PCR array (Human Cell Surface Markers RT² Profiler PCR Array). The analysis showed that CD133⁺ cells expressed specific gene markers of 11 types of cells (*Figure S2B* and *Table S4*). Among them, T-cell marker genes accounted for the highest number of cell-specific genes expressed, with 25 key genes of different T-cell subtypes being detected (*Figure 2B*). To confirm the results of the PCR array, 5 classical markers (CD2, CD3G, CD4, CD8A, and CD8B) of 2 typical T-cell types were selected for detection by real-time PCR. CD133⁺ cells were indeed found to express these T-cell markers (*Figure 2C*). Next, we detected the expression of CD133, CD2, and CD4 in lung adenocarcinoma tissue. Immunohistochemistry (IF) showed that CD133, CD2, and CD4 were expressed on the surface of the cell membrane, and that CD133 was co-expressed with CD2 and CD4 (*Figure 2D*). The results of FCM showed that the levels of CD2⁺, CD4⁺, CD133⁺, CD133⁺CD2⁺, and CD133⁺CD4⁺ cells in cancer tissues were significantly higher

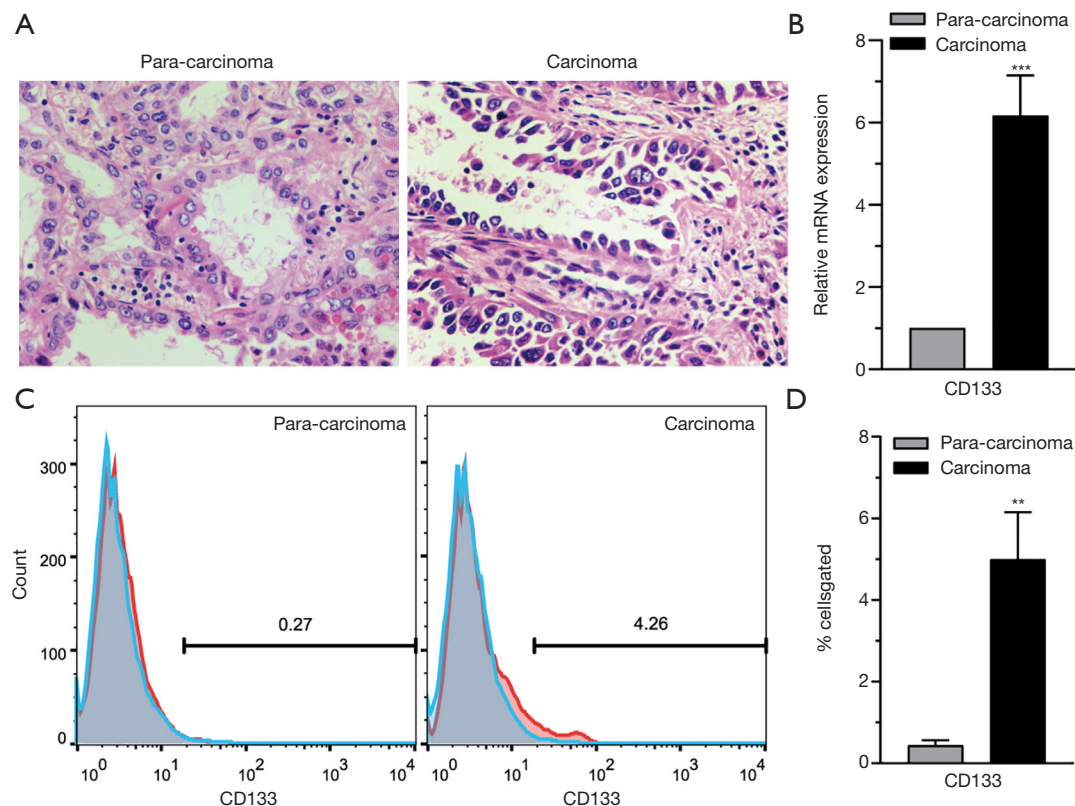


Figure 1 CD133⁺ cells exist in NSCLC. (A) Representative images of H&E staining of carcinoma and para-carcinoma tissues. Magnifications 200x. (B) The expression level of CD133 in 44 tumor tissues examined by real-time PCR. (C) Representative flow cytometry results for CD133 in carcinoma and para-carcinoma tissues from a patient. (D) The expression level of CD133 in 44 tumor tissues examined by flow cytometry. n=44. Data are shown as mean \pm SD. **, P<0.01, ***, P<0.001. NSCLC, non-small cell lung carcinoma; H&E, hematoxylin and eosin; PCR, polymerase chain reaction.

than those in para-carcinoma tissues (Figure 2E,F). These data indicated the presence of CD133⁺CD2⁺ cells in human lung adenocarcinoma. Furthermore, we analyzed the clinical features of 41 NSCLC patients with available clinical data (Table S5) and found a correlation between the presence of CD133⁺CD2⁺ cells and clinicopathological stage (Figure 2G). Our results indicated that CD133⁺CD2⁺ cells are present in NSCLC tumors and may serve as novel malignant markers for patients with NSCLC.

CD133⁺CD2⁺ cells were detected in the A549 cell line

To further confirm the presence of CD133⁺CD2⁺ cancer cells in NSCLC, we detected the levels of these cells in the lung adenocarcinoma cell line A549. FCM analysis performed on A549 cells indicated that the 1.52% of A549 cells were CD133⁺ cells (Figure S3). Then, we enriched

CD133⁺ A549 cells by performing MACS (Figure 3A), and performed a sphere formation assay. The results showed differences in the growth and proliferation of CD133⁺ and CD133⁻ A549 subpopulations (Figure 3B). In addition, the pluripotency factors Sox2, Oct4, and Nanog (22) were highly expressed in CD133⁺ A549 cells compared to CD133⁻ cells (Figure 3C,D,E).

The gene expression profiles of 2 subpopulations were verified with the Human Cell Surface Markers PCR Array. The top 20 genes in the PCR chip of CD133⁺ cells were analyzed, and 75% of them were found to be immune system genes. Of them, T-cell-related genes accounted for the largest proportion (30%) (Figure 3F). This finding also extended our understanding of the differentiation capability of stem-like cells. CD2 is an excellent pan-T-cell marker and 1 of the earliest antigens, appearing on T lymphocytes before CD1 and after CD7. The level of CD2 mRNA in

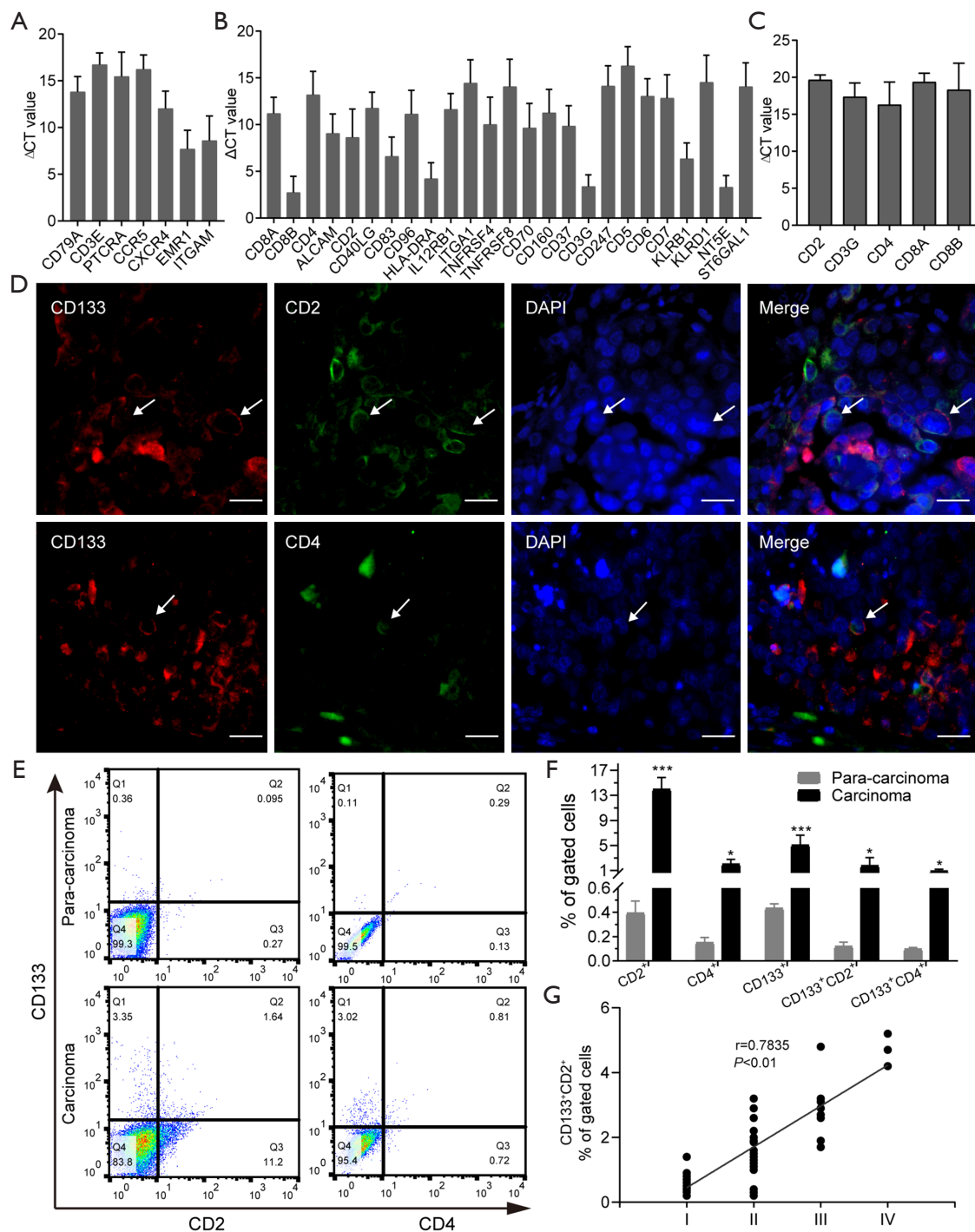


Figure 2 CD133⁺ CD2⁺ cells exist in NSCLC and are correlated with poor prognosis. (A) Gene expression profiles of CD133⁺ cells from tumor tissue by the Human Terminal Differentiation Markers RT² Profiler PCR Array. (B) Gene expression profiles of CD133⁺ cells from tumor tissue by the Human Cell Surface Markers RT² Profiler PCR Array. (C) 5 classical markers of T-cell types detected by real-time PCR. (D) Immunofluorescence staining for CD133, CD2, and CD4 in tumor tissues. Red fluorescence: CD133 molecule. Green fluorescence: CD2 or CD4 molecules. Blue fluorescence: Nucleus. The white arrows refer to the cells co-expressing CD133 with CD2 or CD4. Scale bar: 100 μ m. (E,F) Detection of CD133⁺, CD2⁺, and CD4⁺ cells in tumor tissues by flow cytometry. Data are shown as mean \pm SD. *, $P<0.05$, ***, $P<0.001$. (G) Correlation of CD133⁺ CD2⁺ expression and TNM stage of NSCLC. NSCLC, non-small cell lung carcinoma; PCR, polymerase chain reaction; TNM, tumor node metastasis.

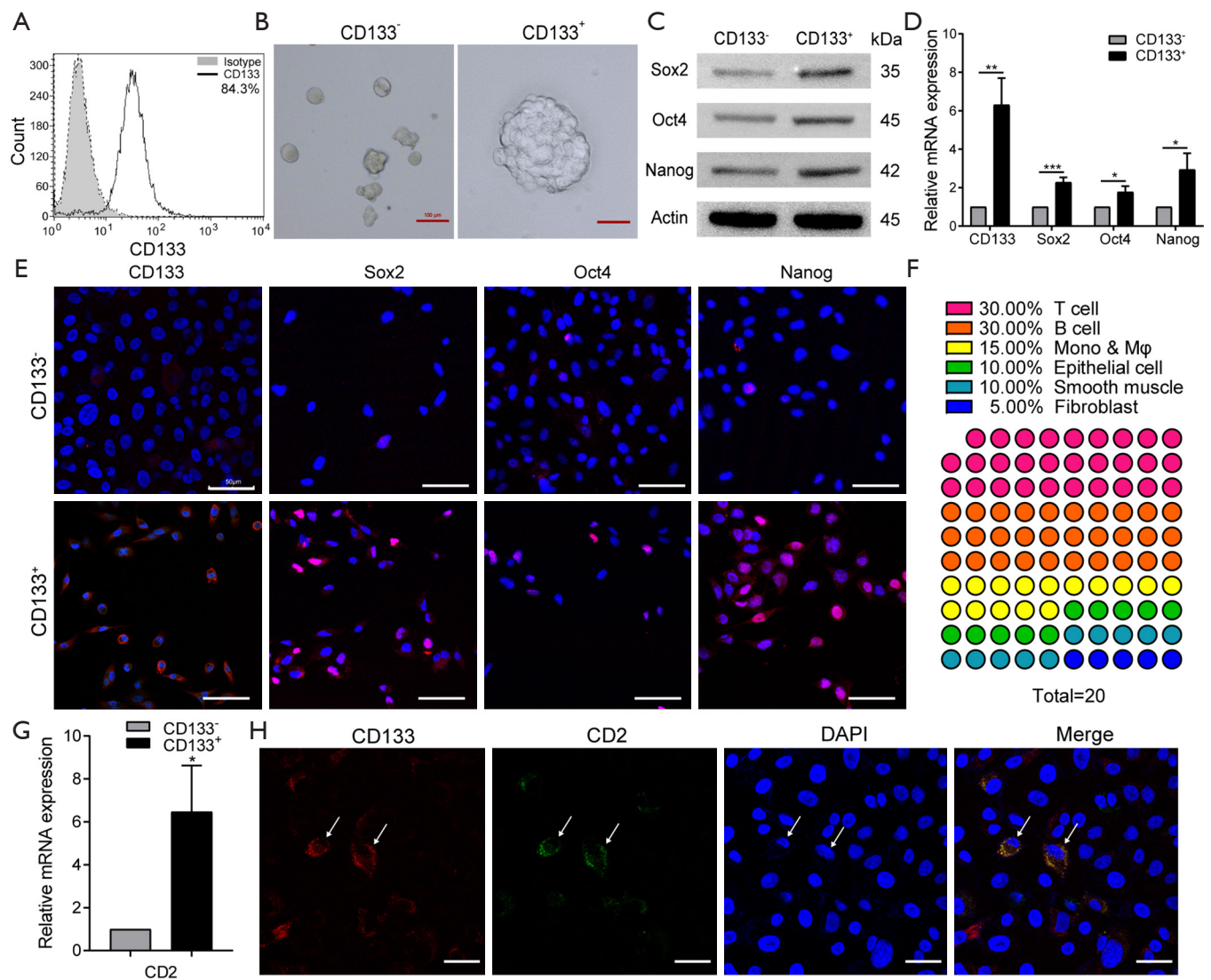


Figure 3 CD133⁺CD2⁺ cells also exist in the A549 cell line. (A) Representative detection of CD133⁺ cells purity after tumor tissues were sorted by MACS. (B) The sphere-forming abilities of CD133⁺ cells and CD133⁻ cells. The pluripotency factors (CD133, Sox2, Oct4, and Nanog) of 2 types of cells were evaluated by western blot (C), real-time PCR (D), and cell immunofluorescence (E). Representative images of western blot and immunofluorescence. Data are presented as the mean \pm SD of 3 replications. Scale bar: 100 μ m. (F) The top 20 genes with the highest expression in CD133⁺ cells in the real-time RT² Profiler PCR Array (Human Cell Surface Markers). (G) Real-time PCR to verify the CD2 expression in both types of cells. (H) Immunofluorescence staining of CD2 (green) and CD133 (red) of CD133⁺ cells. Blue: nucleus. Scale bar: 50 μ m. All data are expressed as the mean \pm SD. *, $P < 0.05$, **, $P < 0.01$, ***, $P < 0.001$. All experiments were repeated at least 3 times. Sox2, SRY-related high-mobility-group (HMG)-box protein-2; Oct4, octamer-binding transcription factor-4; IL-2, interleukin-2; MACS, magnetic-activated cell sorting; PCR, polymerase chain reaction.

both kinds of cells was found to be decreased as tumor cells progressed from CD133⁺ cells to CD133⁻ cells (Figure 3G). The melting curve (Figure S4A), agarose gel electrophoresis (Figure S4B), and sanger sequencing (Figure S4C) indicated it to be a specific amplification. According to all of these

results, CD2 was expressed in A549 cells, and its expression in the CD133⁺ subpopulation was greater than that in CD133⁻ cells. The results of immunofluorescence analyses demonstrated that CD2 could be co-expressed with CD133 on the cytomembrane (Figure 3H). Moreover, CD133⁻ cells

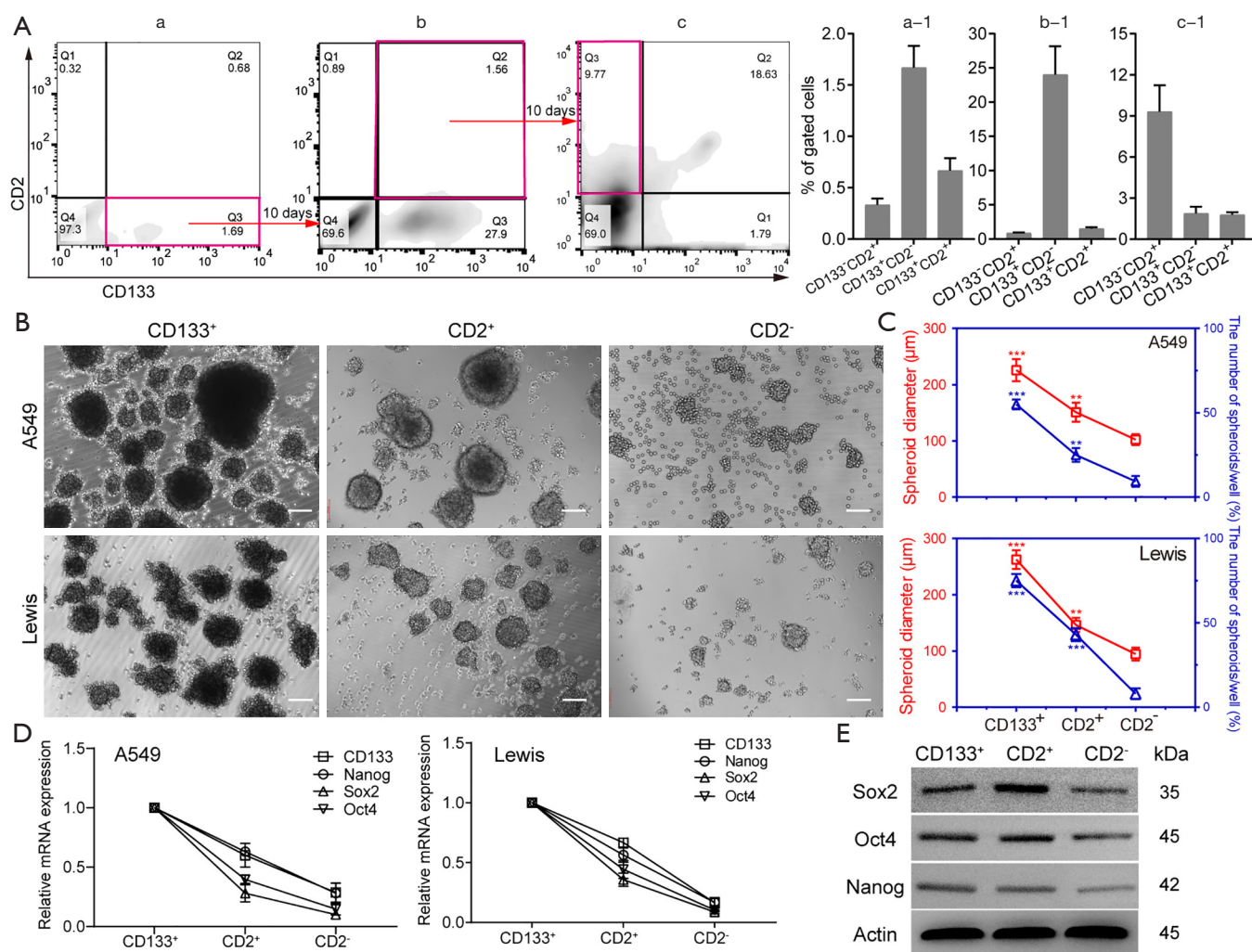


Figure 4 CD2⁺ cells differentiate from CD133⁺ cells and exhibit stronger stem-like properties. (A) The process of CD133⁺ cells differentiation into CD2⁺ cells observed by flow cytometry. The representative result is shown. (B,C) Sphere formation of different types of A549 and Lewis cells, with the sphere-forming capability evaluated based on the spheroid diameter and the number of spheroids. Scale bar: 100 μm. n=5 wells per group. Real-time PCR (D) and western blot (E) detection of pluripotency factors in 3 types of cells. Gene expression was normalized to the geometric mean of the housekeeping gene GAPDH. Data are shown as mean ± SD. All experiments were repeated at least 3 times. **, P<0.01; ***, P<0.001. Sox2, SRY-related high-mobility-group (HMG)-box protein-2; Oct4, octamer-binding transcription factor-4; PCR, polymerase chain reaction.

also expressed CD2 (Figure S5). To sum up, these results suggest that CD133⁺CD2⁺ and CD2⁺ subpopulations exist in the A549 cell line.

CD2⁺ cells differentiated from CD133⁺CD2⁺ cells and exhibited stem-like properties in NSCLC cell line

CD2 is a specific marker for T cells and can therefore be used to identify their presence. Therefore, the identification

of the origin and features of CD2⁺ cells are of considerable interest. Dissociated A549 cells were divided into 4 groups: (I) CD133⁺/CD2⁻, (II) CD133⁺/CD2⁺ (double positive, DP), (III) CD133⁻/CD2⁺, and (IV) CD133⁻/CD2⁻ (double negative, DN) (Figure 4Aa, a-1). To define the lineage potential further, CD133⁺CD2⁻ (Figure 4Aa, Q3) cells were enriched and cultured for 10 days, which resulted in the downregulation of CD133, the upregulation of CD2, and notably, the reappearance of CD133⁺CD2⁺ A549

cells (Figure 4Ab, b-1). Then, we sorted CD133⁺CD2⁺ cells (Figure 4Ab, Q2) by FACS, and the same procedure was performed. After another 10 days, FCM analysis demonstrated the emergence of a CD133⁻CD2⁺ population (Figure 4Ac, Q1 and Figure 4Ac-1). The data confirmed that CD133⁺CD2⁺ progenitors in A549 cells could arise from the CD133⁺ cell population and were capable of differentiating into CD133⁻CD2⁺ cells of tumorous origin. To determine the stem-like properties of CD133⁻CD2⁺ cells, we performed a sphere formation assay. CD2⁺, CD2⁻, and CD133⁺ cells were sorted from A549 and Lewis cell lines by MACS. As shown in Figure 4B, the spheres formed by the 3 kinds of cells displayed different morphological characteristics. Measurement of the diameters and the number of spheroids in each well showed that CD2⁺ cells formed more and larger spheres than CD2⁻ cells but fewer and smaller spheres than CD133⁺ cells (Figure 4C). The expression levels of stemness markers, including CD133, Nanog, Sox2, and Oct4, in CD2⁺ cells were higher than those in CD2⁻ cells but lower than those in CD133⁺ cells (Figure 4D,E). Taken together, our observations indicated that CD2⁺ NSCLC cells exhibited stem-like properties.

CD2⁺ NSCLC cells showed significantly higher proliferation and tumorigenic ability

To evaluate the self-renewal and proliferation of CD2⁺ NSCLC cells *in vitro*, a colony formation assay was conducted. The results showed that the cloning efficiency of CD2⁺ cells was much higher than that of the parent and CD2⁻ cells (Figure 5A,B). We also examined the tumorigenicity of CD2⁺ Lewis cells by injecting C57/BL6 mice with lung carcinoma cells. The effects were evaluated in 3 different groups of mice: the Lewis, CD2⁺ Lewis, and CD2⁻ Lewis. The tumor growth curve and final tumor size data revealed that the average tumor volume and weight in the CD2⁺ group were significantly greater than those in the Lewis and CD2⁻ groups (Figure 5C,D,E). No notable differences in body weight were observed among the mice in the 3 groups (Figure 5F). Ultrasound examination showed that the tumor size of each group started to show a significant difference from 9 days after modeling (Figure 5G). Together, these results indicated that CD2⁺ Lewis cells had strong proliferation ability and were effective in promoting tumor growth.

CD2⁺ NSCLC cell may be a Th17-like cell subpopulation

To further investigate whether CD2⁺ NSCLC cell was T

cell-like, we performed real-time PCR for CD3, a T-cell co-receptor. The 4 chains of CD3 molecules (CD3G, CD3D, CD3E, and CD3Z) were not expressed in CD2⁻ cells. Meanwhile, CD2⁺ cells expressed CD3G at a low level but did not express the other CD3 molecules (Figure 6A). We also analyzed the mRNA levels of CD4 and CD8. CD4 and CD8A were upregulated in CD2⁺ cells compared to CD2⁻ cells (Figure 6B, left). Using the delta CT method after standardization to compare CD8A and CD8B with internal genes, we found that CD8A was expressed in both groups. However, CD8B had an infinite delta CT value, which meant that it was not expressed in the CD2⁺ cells and CD2⁻ cells (Figure 6B, right). Therefore, subsequent experiments focused on CD4⁺ T-cell subsets. Next, we observed the expression of transcription factors and cytokines involved in T-cell polarization. The levels of retinoic acid *ROR γ t* and *interferon regulatory factor 4* (IRF4) genes, which are specific transcription factors of Th17 cells, were significantly higher in CD2⁺ cells (Figure 6C). The same was true for the gene expression of the cytokines IL-17A and IL-22 (Figure 6D), the production of which by Th17 cells triggers inflammatory signaling cascades and increases NSCLC cell proliferation, migration, and invasion (23-25). Subsequently, the secretions of IL-17A and IL-22 in CD2⁺ and CD2⁻ cell culture supernatants were detected by ELISA. After 24 hours of culture, the secretions of IL-17A and IL-22 reached a peak. At 12, 24, and 36 hours after culture, there were significant differences in the IL-17A and IL-22 secretion levels between the CD2⁺ and CD2⁻ groups (Figure 6E). In short, the results of ELISA demonstrated that CD2⁺ cells secreted IL-17A and IL-22. These findings demonstrated that this CD2⁺ subpopulation had a similar phenotype to Th17 lymphocytes (26) and thus, could be referred to as CD2⁺ Th17-like NSCLC cells.

IL-2-mediated phosphorylation of STAT5 suppressed the induction of CD2⁺ Th17-like cells

In the healthy body, IL-2 (27), IL-3 (28), TGF β , and IL-6 are involved in the induction of normal Th17 cell development (29). Therefore, we explored whether these cytokines had a role in CD2⁺ Th17-like cell differentiation. To address this possibility, the expression levels of IL-2, IL-3, IL-6, and TGF β receptors were determined in CD133⁺ subpopulations sorted from A549 cells. IL2R, IL-3R, IL-6R, and TGF β R were observed to be constitutively expressed (Figure 7A). Compared to cells cultured in medium alone, the addition of human IL-2, IL-3, IL-6, and TGF β resulted

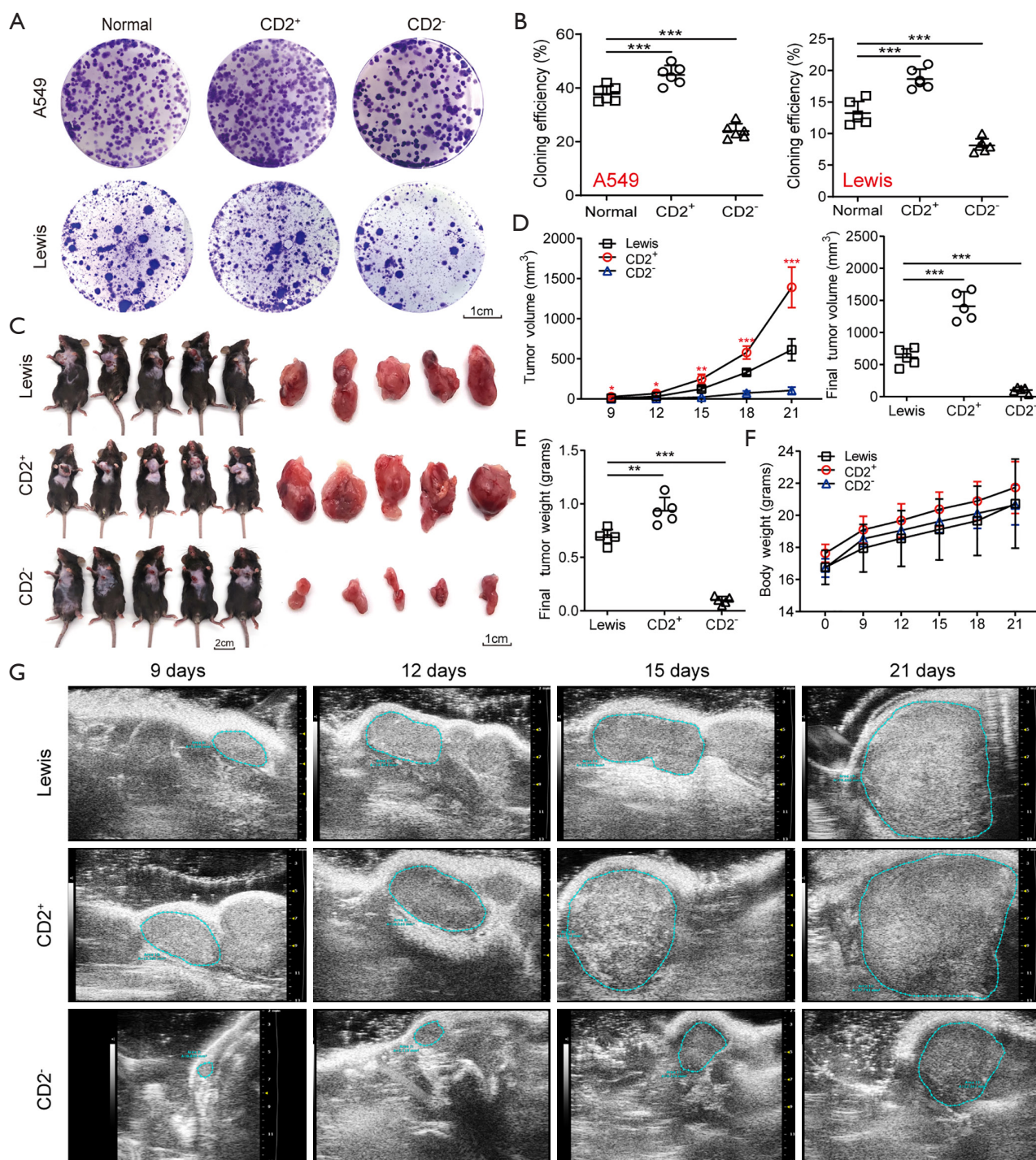


Figure 5 CD2⁺ cells showed strong proliferation ability *in vitro* and *in vivo*. (A,B) Colony formation efficiency of different types of A549 and Lewis cells assessed by colony-forming assay. The colonies were stained with crystal violet dye. Representative images of colonies are shown on panel A. Cloning efficiency of these cells are shown on panel B. Scale bar: 1 cm. n=5 wells per group. (C) Representative images of animal model and tumor samples excised from different groups. (D,E) The average tumor volume and weight of different groups. (F) The average body weight of mice in different groups. (G) Representative ultrasound images of subcutaneously transplanted tumors at different times. n=5 for each group. Data are shown as mean \pm SD. *, P<0.05, **, P<0.01, ***, P<0.001.

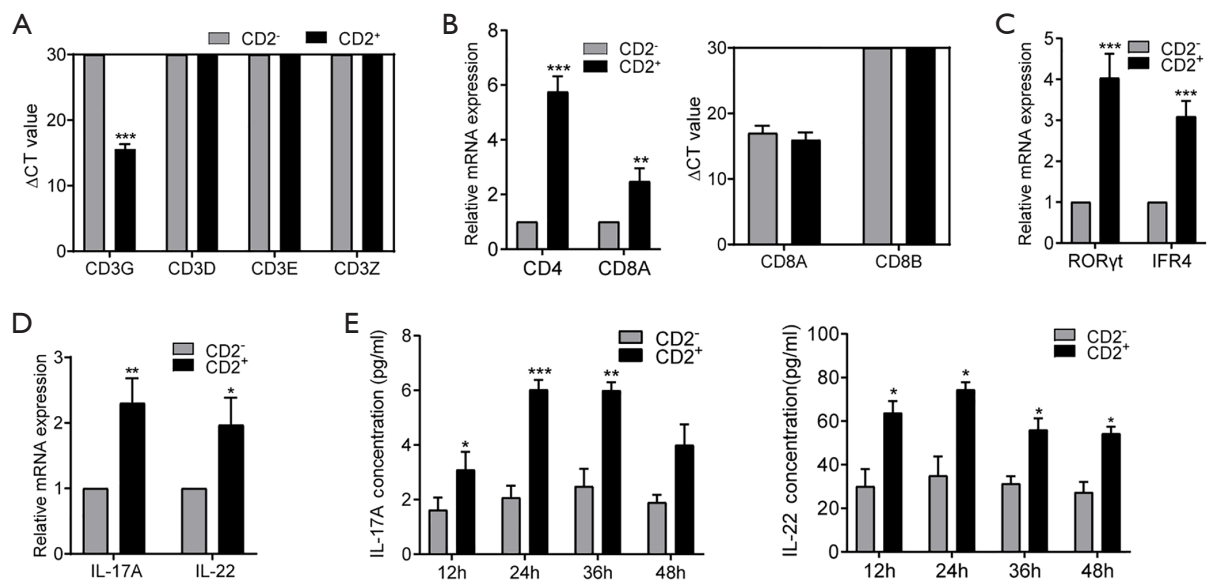


Figure 6 CD2⁺ NSCLC cells may be Th17-like cells. (A,B,C,D) Gene expression levels of the indicated immune markers in CD2⁺ and CD2⁻ cells by real-time PCR. (E) The levels of IL-17 and IL-22 in cell culture supernatants at different times as detected by ELISA. Data are shown as mean ± SD (n=5; *, P<0.05, **, P<0.01, ***, P<0.001). NSCLC, non-small cell lung carcinoma; PCR, polymerase chain reaction; IL, interleukin; ELISA, enzyme-linked immunosorbent assay.

in a marked reduction in the expression of RORγt, IFR4, IL-17A, and IL-22 (Figure 7B). Meanwhile, the results of CCK8 assays showed that cell survival was not affected by IL-2 or IL-3; however, the addition of exogenous IL-6 with TGFβ to the culture promoted the growth of CD133⁺ cells (Figure 7C). Treatment with IL-2 or IL-3 decreased the concentrations of IL-17A and IL-22 in culture supernatant, as determined by ELISA. The inhibitive effect of IL-2 was found to be more significant than that of IL-3, and the inhibition was most obvious after 24 hours of IL-2 treatment (Figure 7D). Therefore, IL-2 was selected as a priority for further study. The results of FCM showed that the addition of IL-2 decreased the proportion of cells expressing IL-17A and RORγt (Figure 7E). These findings revealed that the addition of human IL-2 resulted in a marked reduction in the production of Th17-like cells.

The expression of the orphan nuclear receptor RORγt is widely known to be critical for Th17 differentiation. IL-2 is a potent activator of STAT5 transcription factors that have critical *in vivo* functions in lymphoid development (30). To test whether IL-2 could suppress CD2⁺ Th17-like cell differentiation through an intrinsic cell mechanism requiring STAT5, the effect of exogenous IL-2 on the expression of IL-2R was explored. Data showed that IL-2 acted to promote IL-2R expression (Figure 7F). The level of pSTAT5

was increased and that of RORγt was decreased after IL-2 treatment, whereas the expression of STAT5 was not affected (Figure 7G). This finding supported the hypothesis that IL-2 may suppress CD2⁺ Th17-like cell differentiation via modulation of pSTAT5. To clarify this process, we designed a STAT5 siRNA. As shown in Figure 7H and Figure 7I, the expression of STAT5 was decreased by STAT5 siRNA. The expression levels of RORγt in the STAT5 siRNA and pSTAT5 inhibitor groups were significantly higher than those in the non-transfected and negative control groups (Figure 7J). These observations demonstrated that STAT5 siRNA and pSTAT5 inhibitor reversed the inhibition of RORγt induced by IL-2. In other words, IL-2 inhibited the expression of RORγt via STAT5 phosphorylation. Furthermore, the IL-17A secreted by CD2⁺ Th17-like cells was significantly reduced by the addition of IL-2, and this response was reversed after transfection with STAT5 siRNA or the addition of pSTAT5 inhibitor (Figure 7K). Collectively, these results indicated that IL-2 could inhibit the production of Th17-like cells, possibly via the IL-2R by modulating the phosphorylation level of STAT5. This study demonstrates the multipotency of CD133⁺ cells and their ability to differentiate to CD2⁺ Th17-like cells that promote cancer progression. IL-2-mediated phosphorylation of STAT5 opposes the process of CD133⁺ cells differentiation to CD2⁺

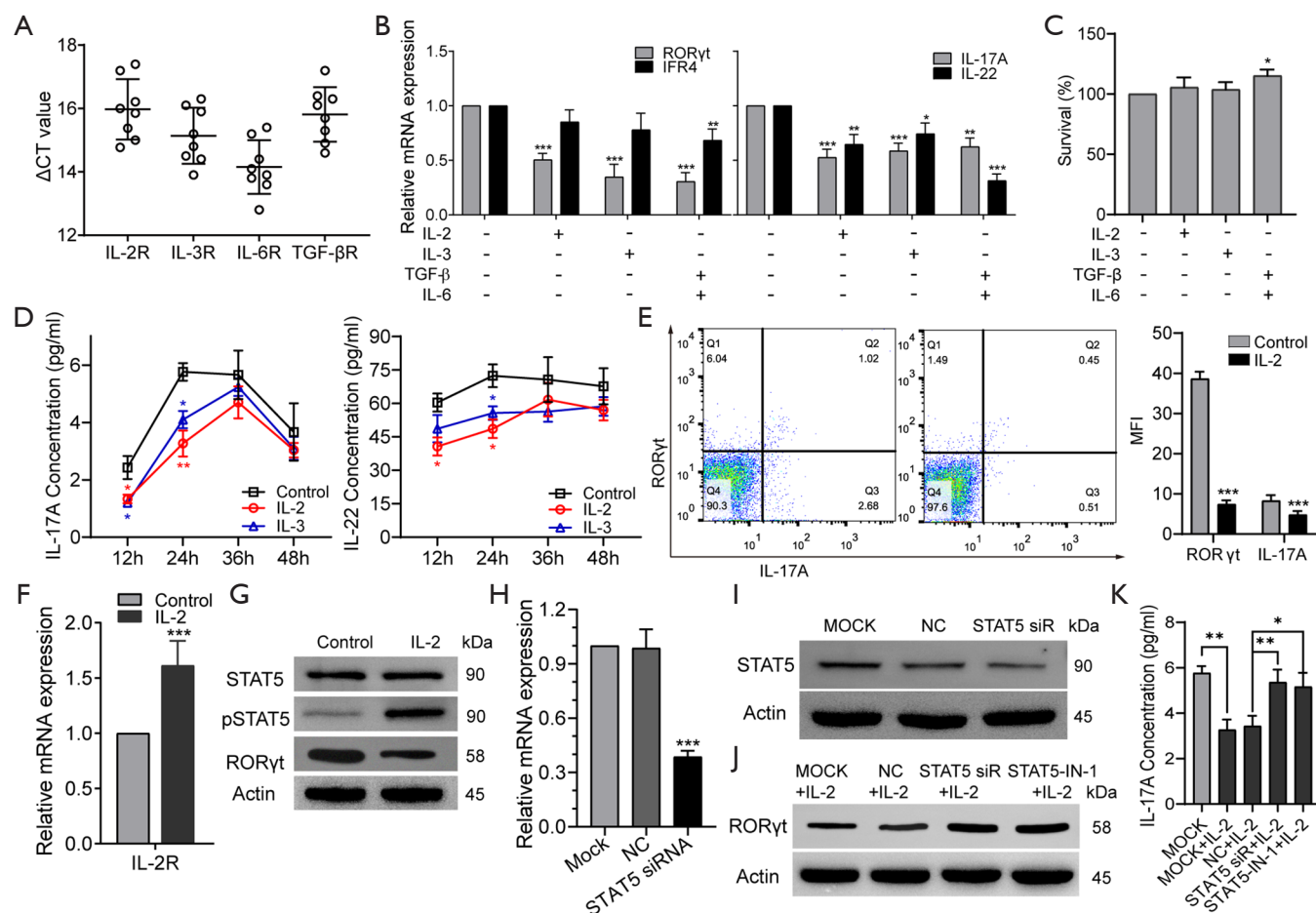


Figure 7 IL-2 can inhibit the production of Th17-like cells by modulating the activation of pSTAT5. (A) The expression of cytokine receptors in CD133⁺ cells by real-time PCR. (B) *RORγt*, *IFR4*, *IL-17A*, and *IL-22* gene expression of CD133⁺ cells in different groups. (C) The survival of CD133⁺ cells were examined by CCK-8 assay. (D) The levels of IL-17A and IL-22 in cell culture supernatants after the indicated treatments at different times as detected by ELISA. (E) Proportions of cells expressing IL-17A and RORγt with the addition of IL-2 as measured by FCM. (F) The levels of IL-2R in CD133⁺ cells after treatment with IL-2 as detected by real-time PCR. (G) Representative western blotting for STAT5, p-STAT5, and RORγt in CD133⁺ cells. (H,I) The significant inhibition of gene and protein expression of STAT5 by STAT5 siRNA. MOCK, solvent control. NC, control siRNA. siRNA, small interfering RNA. (J) Representative western blotting for RORγt. STAT5-IN-1, STAT5 inhibitor. (K) IL-17A expression examined by ELISA. Data represent 3 independent experiments. Data are shown as mean ± SD. *, P<0.05, **, P<0.01, ***, P<0.001. IL, interleukin; TGF-β, transforming growth factor β; RORγt, retinoid-related orphan nuclear receptor γt; STAT5, signal transducer and activator of transcription 5; p-STAT5, Phospho-signal transducer and activator of transcription 5; Th17, T helper cell 17; PCR, polymerase chain reaction; CCK-8, Cell Counting Kit-8; ELISA, enzyme-linked immunosorbent assay; FCM, flow cytometry; IL-2R, IL-2 receptor; siRNA, small interfering RNA.

Th17-like cells. Some other results also suggested that CSCs are multipotent and capable of differentiation along tumor and endothelial lineages, adipocytes, and neurons (Figure 8).

Discussion

The cells in the TME, such as cancer-associated vascular

endothelial cells, fibroblasts, neuroendocrine cells, adipose cells, and immunocytes, are indispensable in all stages of human cancer development, including tumorigenesis, growth, progression, and metastasis (14,16,17,31). Several studies have suggested that CSCs possess multilineage differentiation potential, and they are thought to be the driving factor of intratumoral heterogeneity, cancer

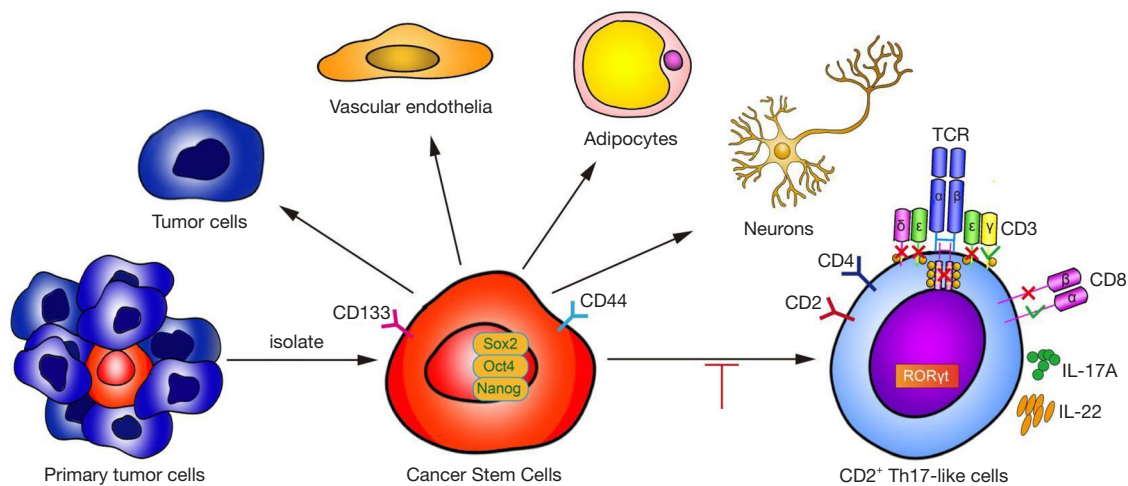


Figure 8 Graphical Abstract. Previous studies have suggested that CSCs are multipotent and capable of differentiation along tumor and endothelial lineages, adipocytes, and neurons. This study demonstrates that CD133⁺ CSCs originating from lung carcinoma differentiate to CD2⁺ Th17-like cells. IL, interleukin; CSCs, cancer stem cells; Th17, T helper cell 17.

metastasis, and therapeutic resistance (4,32). Previous studies have shown that CD133⁺ cells in tumor tissues represent CSCs, while CD133⁻ cells include a complex variety of cells, such as solid tumor cells, infiltrating immune cells, and neovascular endothelial cells (33). To better investigate molecules on the surface and the multi-directional differentiation potential of CSCs, as well as to understand the molecular basis through which CSCs promote tumor progression, we identified and isolated CSCs from NSCLC tissue, indicated by the surface expression of CD133. Our PCR array results showed that CSCs expressed specific genes in 13 tissues, including bone marrow cell-related genes, which suggested that CSCs might create a cellular environment for the tumor that includes tumor-related immune-like cells and is suitable for the survival of tumor cells.

Human T cells can differentiate from bone marrow and mature in the thymus (34), and the relationship between immune cells and tumor cells is extremely important for the development of cancer. We found that a portion of CD133⁺ cells expressed serial markers of immune cells, especially CD2 and CD4. CD133 is a CSCs marker, and CD2 is a surface antigen of the human T-lymphocyte lineage. The subsets of cells expressing both CD133 and CD2 molecules greatly aroused our interest. We found that CD133⁺CD2⁺ cells were present during each stage of NSCLC, and their expression increased along with the tumor grade, suggesting that CD2 together with CD133 may serve as a novel

prognostic predictor for NSCLC patients.

CSCs make up an important portion of the TME; however, CSC differentiation is strictly regulated by the TME and its diverse types of stromal cells and extracellular matrix components (32). We found that CSCs expressed many markers of different types of cells, which comprised the bulk of the TME. Interestingly, the most expressed marker was associated with T cells. T cells play an important role in the antitumor immune response. The earliest marker for T cell differentiation is CD2, which is found on the surface of thymocytes and T cells (35). We found that CD2⁺ cells exhibit stem-like properties in NSCLC cells *in vitro* and promoted the growth of transplanted tumors *in vivo*. Thus, further study of the T-cell subtypes of these CD2⁺ cells and the regulation of their differentiation is of great significance. Many studies have arrived at the conclusion that immune cells are an important component of the TME and play a significant role in the progression of cancers (36). We found that CSCs isolated from an NSCLC cell line could differentiate into CD2⁺ Th17-like immune cells, which indicated that a portion of the immune cells in a TME may originate from CSCs. CD2⁺ Th17-like immune cells secreted the cytokines IL-17A and IL-22, which regulate the proliferation and metastasis of lung cancer cells (24,25). Improved characterization of the immunological properties of CSCs will contribute to the rational design of immunotherapeutic interventions to target these cells and may lead to the eradication of malignant diseases (37).

We demonstrated that CD133⁺ cells can give rise to CD2⁺ Th17-like cells. However, the Th17-like cells showed similar but not identical characteristics to Th17 lymphocytes in the immune system. Specifically, they lacked functional surface markers such as CD3. These CD2⁺ Th17-like cells were found to promote the growth of lung carcinoma cells. Further investigation is needed to fully demonstrate the specific functions of CD133⁺-derived CD2⁺ Th17-like cells. These CD2⁺ Th17-like cells may be one of the components of the blood–tumor barrier and act as a tumor immune guard. We speculate that the Th17-like cells can recognize and tolerate the tumor cells because they share the same origin, which may help tumor cells to complete the immune escape process. All of these possibilities are worthy of further study.

Inhibiting the production of Th17-like cells may be an effective approach for NSCLC therapy. We found that IL-2 inhibited the production of Th17-like cells, acting through the IL-2R by modulating the activation of STAT5 signaling.

Our research provides direct evidence that the CD2⁺ Th17-like tumor-related immune-like cells differentiate from CD133⁺ CSCs through an intermediate CD133⁺CD2⁺ progenitor cell and support cancer progression. Not only do these findings enrich the definition of the multidirectional differentiation potential of CSCs but from them, we can also infer that the inhibitory TME forms a blood-tumor barrier, which protects the tumor cells as the blood-brain barrier protects nerve cells (38) and as the placental barrier protects the fetus (39). This barrier is not only difficult for immune cells to overcome, but it is also hard for some macromolecule-targeted drugs to penetrate. However, how CSCs participate in the construction of the TME remains complex, and additional experiments and clinical studies are needed in the future.

Acknowledgments

We thank Huaxing Zhang for providing assistance with this study, and LetPub (www.letpub.com) for providing linguistic assistance during the preparation of this manuscript.

Funding: This work was supported by the Colleges and Universities in Hebei Province Scientific Research Project High Level Talents Fund (No. GCC2014004), the CAMS Innovation Fund for Medical Sciences (2019-12M-5-055), Natural Science Foundation of Hebei Province (H2020206579), and the Key Research and Development Program of Hebei Province (20327125D).

Footnote

Reporting Checklist: The authors have completed the ARRIVE reporting checklist. Available at <http://dx.doi.org/10.21037/atm-21-980>

Data Sharing Statement: Available at <http://dx.doi.org/10.21037/atm-21-980>

Conflicts of Interest: All authors have completed the ICMJE uniform disclosure form (available at <http://dx.doi.org/10.21037/atm-21-980>). The authors have no conflicts of interest to declare.

Ethical Statement: The authors are accountable for all aspects of the work in ensuring that questions related to the accuracy or integrity of any part of the work are appropriately investigated and resolved. This study conformed to the provisions of the Declaration of Helsinki (as revised in 2013). Informed written consent was obtained from all the patients involved in the study and the protocol was approved by the medical ethics committee of Hebei Medical University (No. 20190066). All animal experiments were performed according to the Guidelines for the Care and Use of Laboratory Animals. The experimental protocols were approved by the Local Committee on Animal Care, Use and Protection of Hebei Medical University. The approval file for study related to animal experiment was No. 20190051.

Open Access Statement: This is an Open Access article distributed in accordance with the Creative Commons Attribution-NonCommercial-NoDerivs 4.0 International License (CC BY-NC-ND 4.0), which permits the non-commercial replication and distribution of the article with the strict proviso that no changes or edits are made and the original work is properly cited (including links to both the formal publication through the relevant DOI and the license). See: <https://creativecommons.org/licenses/by-nc-nd/4.0/>.

References

1. Bray F, Ferlay J, Soerjomataram I, et al. Global cancer statistics 2018: GLOBOCAN estimates of incidence and mortality worldwide for 36 cancers in 185 countries. *CA Cancer J Clin* 2018;68:394-424.
2. Guilbaud E, Gautier EL, Yvan-Charvet L. Macrophage Origin, Metabolic Reprogramming and IL-1 Signaling:

- Promises and Pitfalls in Lung Cancer. *Cancers (Basel)* 2019;11:298.
3. Schegoleva AA, Khozyainova AA, Fedorov AA, et al. Prognosis of Different Types of Non-Small Cell Lung Cancer Progression: Current State and Perspectives. *Cell Physiol Biochem* 2021;55:29-48.
 4. Makena MR, Ranjan A, Thirumala V, et al. Cancer stem cells: Road to therapeutic resistance and strategies to overcome resistance. *Biochim Biophys Acta Mol Basis Dis* 2020;1866:165339.
 5. Ghasemi F, Sarabi PZ, Athari SS, et al. Therapeutics strategies against cancer stem cell in breast cancer. *Int J Biochem Cell Biol* 2019;109:76-81.
 6. Giraldo NA, Sanchez-Salas R, Peske JD, et al. The clinical role of the TME in solid cancer. *Br J Cancer* 2019;120:45-53.
 7. Chen J, Zhou R. Tumor microenvironment related novel signature predict lung adenocarcinoma survival. *PeerJ* 2021;9:e10628.
 8. Kim JM, Chen DS. Immune escape to PD-L1/PD-1 blockade: seven steps to success (or failure). *Ann Oncol* 2016;27:1492-504.
 9. Relation T DM, Horwitz EM. Concise Review An (Im) Penetrable Shield How the Tumor Microenvironment Protects Cancer Stem Cells. *Stem Cells* 2017;35:1123-30.
 10. Murad JP, Tilakawardane D, Park AK, et al. Pre-conditioning modifies the TME to enhance solid tumor CAR T cell efficacy and endogenous protective immunity. *Mol Ther* 2021. [Epub ahead of print]. doi: 10.1016/j.jymthe.2021.02.024.
 11. Huang H, Fang J, Fan X, et al. Advances in Molecular Mechanisms for Traditional Chinese Medicine Actions in Regulating Tumor Immune Responses. *Front Pharmacol* 2020;11:1009.
 12. Wu HJ, Chu PY. Role of Cancer Stem Cells in Cholangiocarcinoma and Therapeutic Implications. *Int J Mol Sci* 2019;20:4154.
 13. Garg M. Epithelial Plasticity, Autophagy and Metastasis: Potential Modifiers of the Crosstalk to Overcome Therapeutic Resistance. *Stem Cell Rev Rep* 2020;16:503-10.
 14. Wang R, Chadalavada K, Wilshire J, et al. Glioblastoma stem-like cells give rise to tumour endothelium. *Nature* 2010;468:829-33.
 15. Shangguan W, Fan C, Chen X, et al. Endothelium originated from colorectal cancer stem cells constitute cancer blood vessels. *Cancer Sci* 2017;108:1357-67.
 16. Ishay-Ronen D, Diepenbruck M, Kalathur RKR, et al. Gain Fat-Lose Metastasis: Converting Invasive Breast Cancer Cells into Adipocytes Inhibits Cancer Metastasis. *Cancer Cell* 2019;35:17-32.e6.
 17. Lu R, Fan C, Shangguan W, et al. Neurons generated from carcinoma stem cells support cancer progression. *Signal Transduct Target Ther* 2017;2:16036.
 18. Jia X, Cong B, Zhang J, et al. CCK8 negatively regulates the TLR9-induced activation of human peripheral blood pDCs by targeting TRAF6 signaling. *Eur J Immunol* 2014;44:489-99.
 19. Zhou W, Chen X, Hu Q, et al. Galectin-3 activates TLR4/NF-kappaB signaling to promote lung adenocarcinoma cell proliferation through activating lncRNA-NEAT1 expression. *BMC Cancer* 2018;18:580.
 20. Kim WT, Ryu CJ. Cancer stem cell surface markers on normal stem cells. *BMB Rep* 2017;50:285-98.
 21. Vora P, Venugopal C, Salim SK, et al. The Rational Development of CD133-Targeting Immunotherapies for Glioblastoma. *Cell Stem Cell* 2020;26:832-44.e6.
 22. Balaji S, Santhi R, Kim U, et al. Cancer Stem Cells with Overexpression of Neuronal Markers Enhance Chemoresistance and Invasion in Retinoblastoma. *Curr Cancer Drug Targets* 2020;20:710-9.
 23. Wang D, Yu W, Lian J, et al. Th17 cells inhibit CD8(+) T cell migration by systematically downregulating CXCR3 expression via IL-17A/STAT3 in advanced-stage colorectal cancer patients. *J Hematol Oncol* 2020;13:68.
 24. Li H, Zhang Q, Wu Q, et al. Interleukin-22 secreted by cancer-associated fibroblasts regulates the proliferation and metastasis of lung cancer cells via the PI3K-Akt-mTOR signaling pathway. *Am J Transl Res* 2019;11:4077-88.
 25. Wu Z, He D, Zhao S, et al. IL-17A/IL-17RA promotes invasion and activates MMP-2 and MMP-9 expression via p38 MAPK signaling pathway in non-small cell lung cancer. *Mol Cell Biochem* 2019;455:195-206.
 26. Liu W, Li H, Zhang X, et al. Prostaglandin I2-IP signalling regulates human Th17 and Treg cell differentiation. *Prostaglandins Leukot Essent Fatty Acids* 2013;89:335-44.
 27. Alam F, Singh A, Flores-Malavet V, et al. CD25-Targeted IL-2 Signals Promote Improved Outcomes of Influenza Infection and Boost Memory CD4 T Cell Formation. *J Immunol* 2020;204:3307-14.
 28. Jahandideh B, Derakhshani M, Abbaszadeh H, et al. The pro-Inflammatory cytokines effects on mobilization, self-renewal and differentiation of hematopoietic stem cells. *Hum Immunol* 2020;81:206-17.
 29. Martinez-Sanchez ME, Mendoza L, Villarreal C, et

- al. A Minimal Regulatory Network of Extrinsic and Intrinsic Factors Recovers Observed Patterns of CD4+ T Cell Differentiation and Plasticity. *PLoS Comput Biol* 2015;11:e1004324.
30. Bauché D, Joyce-Shaikh B, Fong J, et al. IL-23 and IL-2 activation of STAT5 is required for optimal IL-22 production in ILC3s during colitis. *Sci Immunol* 2020;5:eaav1080.
 31. Begum A, McMillan RH, Chang YT, et al. Direct Interactions With Cancer-Associated Fibroblasts Lead to Enhanced Pancreatic Cancer Stem Cell Function. *Pancreas* 2019;48:329-34.
 32. Saijo A, Goto H, Nakano M, et al. Bone marrow-derived fibrocytes promote stem cell-like properties of lung cancer cells. *Cancer Lett* 2018;421:17-27.
 33. Chen E, Zeng Z, Bai B, et al. The prognostic value of CSCs biomarker CD133 in NSCLC: a meta-analysis. *Oncotarget* 2016;7:56526-39.
 34. Terstappen LW, Huang S, Picker LJ. Flow cytometric assessment of human T-cell differentiation in thymus and bone marrow. *Blood* 1992;79:666-77.
 35. Cho DH, Kim MC, Park CI. Expression analysis data of T-cell surface antigen CD2 gene from rock bream (*Oplegnathus fasciatus*). *Data Brief* 2019;24:103832.
 36. Varn FS, Wang Y, Mullins DW, et al. Systematic Pan-Cancer Analysis Reveals Immune Cell Interactions in the Tumor Microenvironment. *Cancer Res* 2017;77:1271-82.
 37. Harjes U. Tumour immunology: Tumours copy to escape. *Nat Rev Cancer* 2017;17:453.
 38. Bar-Klein G, Lublinsky S, Kamintsky L, et al. Imaging blood-brain barrier dysfunction as a biomarker for epileptogenesis. *Brain* 2017;140:1692-705.
 39. Muoth C, Aengenheister L, Kucki M, et al. Nanoparticle transport across the placental barrier: pushing the field forward! *Nanomedicine (Lond)* 2016;11:941-57.

Cite this article as: Jia M, Jia X, Zhang D, Liu W, Yi S, Li Z, Cong B, Ma C, Li S, Zhang J. CD2⁺ T-helper 17-like cells differentiated from a CD133⁺ subpopulation of non-small cell lung carcinoma cells promote the growth of lung carcinoma. *Ann Transl Med* 2021;9(8):687. doi: 10.21037/atm-21-980

Table S1 Antibodies Information

Name	Vendor	Catalog
Oct-4 Antibody	Cell Signaling	2750
Sox2 (D6D9) XP® Rabbit mAb	Cell Signaling	3579
Nanog (D73G4) XP® Rabbit mAb	Cell Signaling	4903
FITC Mouse Anti-Human CD2	BD Biosciences	555326
FITC Mouse Anti-Human CD4	BD Biosciences	550628
FITC Mouse IgG1, κ Isotype Control	BD Biosciences	555748
CD133/1 Antibody, anti-human, APC	Miltenyi Biotec	130-113-668
Isotype control antibodies, mouse IgG1, APC	Miltenyi Biotec	130-113-196
Octamer-binding transcription factor-4 (Oct4) Antibody	Cell Signaling	2750
SRY-related high-mobility-group (HMG)-box protein-2 (Sox2) (D6D9) XP® Rabbit mAb	Cell Signaling	3579
Nanog (D73G4) XP® Rabbit mAb	Cell Signaling	4903
Signal transducer and activator of transcription protein 5 (Stat5) (D3N2B) Rabbit mAb	Cell Signaling	25656
Phospho-Stat5 (Tyr694) (D47E7) XP® Rabbit mAb	Cell Signaling	4322
Retinoic acid receptor-related orphan receptor gamma t (ROR γ t) Monoclonal Antibody	Invitrogen	14-6988-82
β -Actin	Cell Signaling	4970
Rabbit Anti-CD133 antibody	Abcam	ab19898
Mouse Anti-CD2 antibody	Abcam	ab193344
Mouse Anti-CD4 antibody	Abcam	ab25804
Alexa Fluor 488 Goat anti-Mouse IgG antibody	Invitrogen	A-21121
Alexa Fluor 594 Goat anti-Rabbit IgG antibody	Invitrogen	R37117

Table S2 Primers used for qRT-PCR

Gene	Forward primer (5' to 3')	Reverse primer (5' to 3')
ACTB	TGACCCAGATCATGTTTGAG	CGTACAGGGATAGCACAG
CD2	AGCCTGAGTGCAAAATTCAAGT	AAAACGAGCAGTGCCACAAAG
CD4	TGCCTCAGTATGCTGGCTCT	GAGACCTTTGCCTCCTTGTTT
CD8A	TCCTCCTATACCTCTCCCAAAAC	GGAAGACCGGCACGAAGTG
CD8B	TCAATCTCACAAGCGTGAAGC	GGTAACCGGCACACTCTCTT
ROR γ t	GTGGGGACAAGTCGTCTGG	AGTGCTGGCATCGGTTTCG
IRF4	AAAGGAAAGTTCCGAGAAGG	CGAAGGGTAAGGCGTTGT
IL-17A	AGATTACTACAACCGATCCACCT	GGGGACAGAGTTCATGTGGTA
IL-23	CTCAGGGACAACAGTCAGTTC	ACAGGGCTATCAGGGAGCA
CD3G	GGAATCTGGGAAGTAATGCCAA	TCAATGCAGTCTGACACATTCT
CD3D	ACTGGCTACCCTTCTCTCG	CCGTTCCCTCTACCCATGTGA
CD3E	CCTCTTATCAGTTGGCGTTTGG	TTCAGTGACAGGTGATCCTCA
CD3Z	GGCACAGTTGCCGATTACAGA	CTGCTGAACTTCACTCTCAGG
CD56	GGCATTTACAAGTGTGTGGTTAC	TTGGCGCATTCTTGAACATGA
CD19	CCAGAACCAGTACGGGAACG	CTCGGGTTTCCATAAGACGGG
CD14	GACCTAAAGATAACCGGCACC	GCAATGCTCAGTACCTTGAGG
CD31	CCAAGGTGGGATCGTGAGG	TCGGAAGGATAAAACGCGGTC
CD133 (homo)	AGTCGGAAACTGGCAGATAGC	GGTAGTGTTGACTGGGCCAAT
CD133 (mouse)	ACTGGGGCTGTGTGGAAAG	GCATTGAAGGTATCTTGGGTCTC
Nanog (homo)	TTTGTGGGCCTGAAGAAAAC	AGGGCTGTCTGAATAAGCAG
Nanog (mouse)	CACAGTTTGCCTAGTTCTGAGG	GCAAGAATAGTTCTCGGGATGAA
Sox2 (homo)	GCCGAGTGGAAACTTTTGTCC	GGCAGCGTGTACTTATCCTTCT
Sox2 (mouse)	GCGGAGTGGAAACTTTTGTCC	GGGAAGCGTGTACTTATCCTTCT
Oct4 (homo)	CTTGAATCCCGAATGGAAGGG	GTGTATATCCAGGGTGATCCTC
Oct4 (mouse)	AGAGGATCACCTTGGGGTACA	CGAAGCGACAGATGGTGGTC
IL-2R	CAGCGGTGAATGGCACTTC	GGCATGGACTTGGCAGGAA
IL-3R	ACGAAGGAAGATCCAAACCCA	GCATAGAATAGTCGGCGTCTTTA
IL-6R	CCCCTCAGCAATGTTGTTTGT	CTCCGGGACTGTAACTGG
TGF β R	GTAGCTCTGATGAGTGCAATGAC	CAGATATGGCAACTCCCAGTG
STAT5	GCAGAGTCCGTGACAGAGG	CCACAGGTAGGGACAGAGTCT

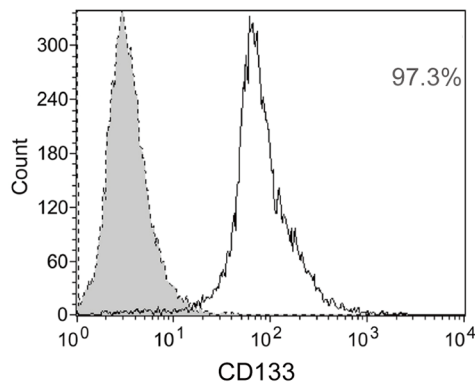


Figure S1 Representative detection of CD133⁺ cell purity after tumor tissues were sorted by FACS. FACS, fluorescence-activated cell sorting.

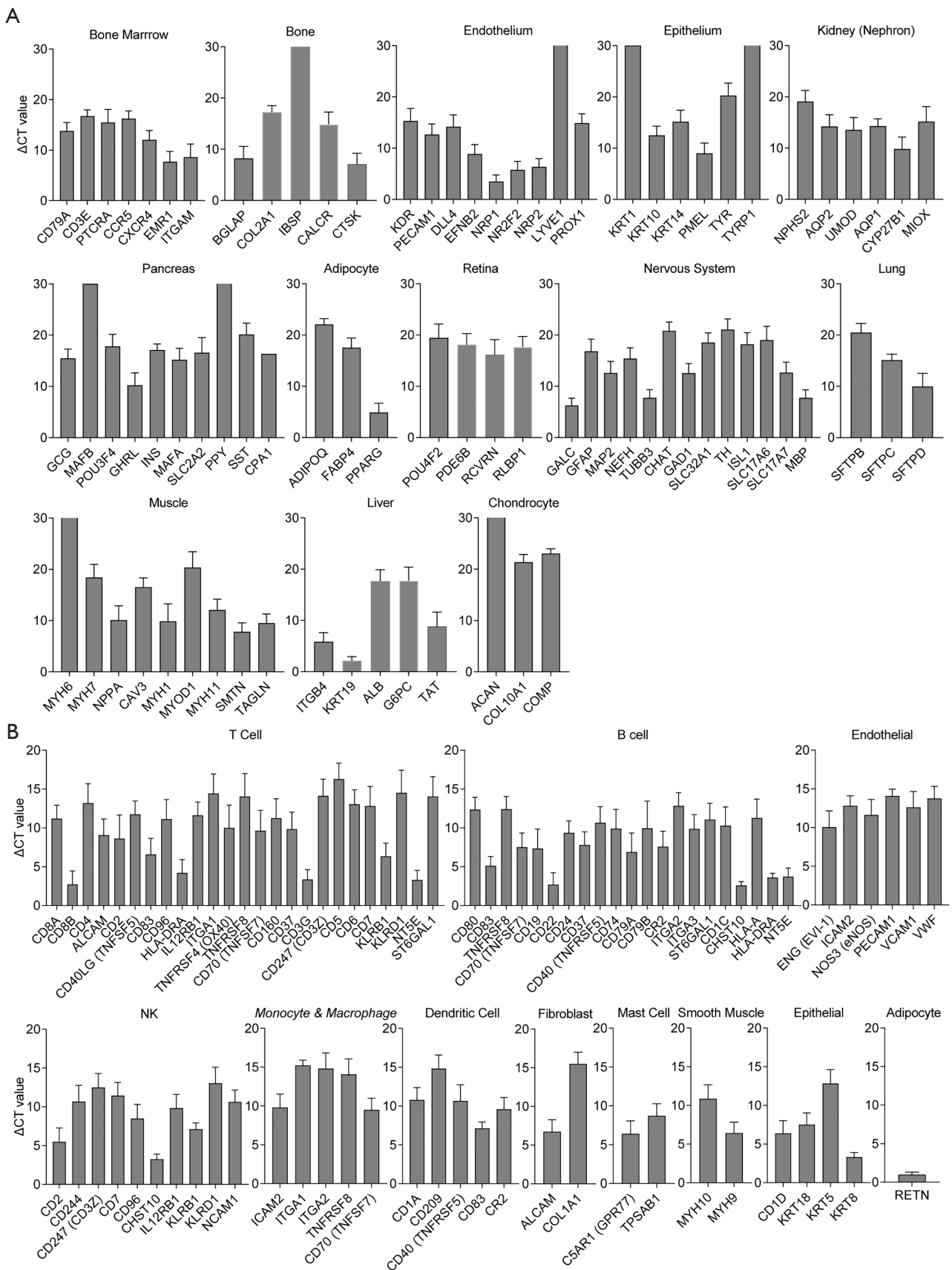


Figure S2 Gene expression profiles of the CD133⁺ cells from NSCLC tissue. (A) Gene expression profile of CD133⁺ CSCs by Human Terminal Differentiation Markers RT² Profiler PCR Array. (B) Gene expression profile of CD133⁺ cells by Human Cell Surface Markers RT² Profiler PCR Array. Data are shown as mean \pm SD. NSCLC, non-small cell lung carcinoma; CSCs, cancer stem cells; PCR, polymerase chain reaction.

Table S3 Terminal Differentiation Markers RT² Profiler PCR Array

Tissues type	Gene list
Adipocytes	ADIPOQ(ACRP30), FABP4, PPARG
Chondrocytes	ACAN, COL10A1, COMP
Endothelium	
General endothelium	CDH5, KDR (VEGFR3), PECAM1
Arterial endothelium	DLL4, EFNB2, NRP1
Lymphatic endothelium	LYVE1, PROX1
Venous endothelium	NR2F2, NRP2
Epithelium	
Keratinocyte epithelium	KRT1, KRT10, KRT14
Melanocyte epithelium	PMEL, TYR, TYRP1
Bone cells	
Osteoblasts	BGLAP, COL2A1, IBSP
Osteoclasts	CALCR, CTSK
Liver cells	
Cholangiocytes	ITGB4, KRT19
Hepatocytes	ALB, G6PC, TAT
Bone marrow cells	
Early B-Cell development	CD79A
Early T-Cell development	CD3E, PTCRA
Macrophages	ADGRE1 (EMR1), CCR5, CXCR4
Monocytes	ITGAM
Nervous system cells	
Glial cells	GALC, GFAP
Mature neurons	MAP2, NEFH, TUBB3
Cholinergic neurons	CHAT
Dopaminergic neurons	TH
GABA neurons	GAD1, SLC32A1
Glutamatergic neurons	SLC17A6, SLC17A7
Motor neurons	ISL1
Oligodendrocytes	MBP
Retinal cells	
Ganglion cells	POU4F2
Muller cells	RLBP1
Photoreceptor cells	PDE6B, RCVRN
Nephrons	
Podocytes	NPHS2
Proximal tubule cells	AQP1, CYP27B1, MIOX
Collecting duct cells	AQP2
Distal tubule cells	UMOD
Lung cells	SFTPB, SFTPC, SFTPD
Muscle cells	
Cardiomyocytes	MYH6, MYH7, NPPA
Skeletal muscle Cells	CAV3, MYH1, MYOD1
Smooth muscle Cells	MYH11, SMTN, TAGLN
Pancreatic cells	
Alpha cells	GCG, MAFB, POU3F4
Beta cells	INS, MAFA, SLC2A2
Delta cells	SST
Epsilon cells	GHRL (Ghrelin, Obestatin)
Pancreatic polypeptide-producing (PP) cells	PPY
Exocrine cells	CPA1

Gene Description

GenBank	Symbol	Description
NM_001135	ACAN	Aggrecan
NM_004797	ADIPOQ	Adiponectin, C1Q and collagen domain containing
NM_000477	ALB	Albumin
NM_198098	AQP1	Aquaporin 1 (Colton blood group)
NM_000486	AQP2	Aquaporin 2 (collecting duct)
NM_199173	BGLAP	Bone gamma-carboxyglutamate (gla) protein
NM_001742	CALCR	Calcitonin receptor
NM_001234	CAV3	Caveolin 3
NM_000579	CCR5	Chemokine (C-C motif) receptor 5
NM_000733	CD3E	CD3e molecule, epsilon (CD3-TCR complex)
NM_001783	CD79A	CD79a molecule, immunoglobulin-associated alpha
NM_001795	CDH5	Cadherin 5, type 2 (vascular endothelium)
NM_020985	CHAT	Choline O-acetyltransferase
NM_000493	COL10A1	Collagen, type X, alpha 1
NM_001844	COL2A1	Collagen, type II, alpha 1
NM_000095	COMP	Cartilage oligomeric matrix protein
NM_001868	CPA1	Carboxypeptidase A1 (pancreatic)
NM_000396	CTSK	Cathepsin K
NM_003467	CXCR4	Chemokine (C-X-C motif) receptor 4
NM_000785	CYP27B1	Cytochrome P450, family 27, subfamily B, polypeptide 1
NM_019074	DLL4	Delta-like 4 (Drosophila)
NM_004093	EFNB2	Ephrin-B2
NM_001974	EMR1	Egf-like module containing, mucin-like, hormone receptor-like 1
NM_001442	FABP4	Fatty acid-binding protein 4, adipocyte
NM_000151	G6PC	Glucose-6-phosphatase, catalytic subunit
NM_000817	GAD1	Glutamate decarboxylase 1 (brain, 67kDa)
NM_000153	GALC	Galactosylceramidase
NM_002054	GCG	Glucagon
NM_002055	GFAP	Glial fibrillary acidic protein
NM_016362	GHRL	Ghrelin/obestatin prepropeptide
NM_004967	IBSP	Integrin-binding sialoprotein
NM_000207	INS	Insulin
NM_002202	ISL1	ISL LIM homeobox 1
NM_000632	ITGAM	Integrin, alpha M (complement component 3 receptor 3 subunit)
NM_000213	ITGB4	Integrin, beta 4
NM_002253	KDR	Kinase insert domain receptor (a type III receptor tyrosine kinase)
NM_006121	KRT1	Keratin 1
NM_000421	KRT10	Keratin 10
NM_000526	KRT14	Keratin 14
NM_002276	KRT19	Keratin 19
NM_006691	LYVE1	Lymphatic vessel endothelial hyaluronan receptor 1
NM_201589	MAFA	V-maf musculoaponeurotic fibrosarcoma oncogene homolog A (avian)
NM_005461	MAFB	V-maf musculoaponeurotic fibrosarcoma oncogene homolog B (avian)
NM_002374	MAP2	Microtubule-associated protein 2
NM_002385	MBP	Myelin basic protein
NM_017584	MIOX	Myo-inositol oxygenase
NM_005963	MYH1	Myosin, heavy chain 1, skeletal muscle, adult
NM_022844	MYH11	Myosin, heavy chain 11, smooth muscle
NM_002471	MYH6	Myosin, heavy chain 6, cardiac muscle, alpha
NM_000257	MYH7	Myosin, heavy chain 7, cardiac muscle, beta
NM_002478	MYOD1	Myogenic differentiation 1
NM_021076	NEFH	Neurofilament, heavy polypeptide
NM_014625	NPHS2	Nephrosis 2, idiopathic, steroid-resistant (podocin)
NM_006172	NPPA	Natriuretic peptide A
NM_021005	NR2F2	Nuclear receptor subfamily 2, group F, member 2
NM_003873	NRP1	Neuropilin 1
NM_003872	NRP2	Neuropilin 2
NM_000283	PDE6B	Phosphodiesterase 6B, cGMP-specific, rod, beta
NM_000442	PECAM1	Platelet/endothelial cell adhesion molecule
NM_006928	PMEL	Premelanosome protein
NM_000307	POU3F4	POU class 3 homeobox 4
NM_004575	POU4F2	POU class 4 homeobox 2
NM_015869	PPARG	Peroxisome proliferator-activated receptor gamma
NM_002722	PPY	Pancreatic polypeptide
NM_002763	PROX1	Prospero homeobox 1
NM_138296	PTCRA	Pre T-cell antigen receptor alpha
NM_002903	RCVRN	Recoverin
NM_000326	RLBP1	Retinaldehyde-binding protein 1
NM_000542	SFTPB	Surfactant protein B
NM_003018	SFTPC	Surfactant protein C
NM_003019	SFTPD	Surfactant protein D
NM_020346	SLC17A6	Solute carrier family 17 (sodium-dependent inorganic phosphate cotransporter), member 6
NM_020309	SLC17A7	Solute carrier family 17 (sodium-dependent inorganic phosphate cotransporter), member 7
NM_000340	SLC2A2	Solute carrier family 2 (facilitated glucose transporter), member 2
NM_080552	SLC32A1	Solute carrier family 32 (GABA vesicular transporter), member 1
NM_006932	SMTN	Smoothelin
NM_001048	SST	Somatostatin
NM_003186	TAGLN	Transgelin
NM_000353	TAT	Tyrosine aminotransferase
NM_000360	TH	Tyrosine hydroxylase
NM_006086	TUBB3	Tubulin, beta 3
NM_000372	TYR	Tyrosinase (oculocutaneous albinism IA)
NM_000550	TYRP1	Tyrosinase-related protein 1
NM_003361	UMOD	Uromodulin
NM_001101	ACTB	Actin, beta
NM_004048	B2M	Beta-2-microglobulin
NM_002046	GAPDH	Glyceraldehyde-3-phosphate dehydrogenase
NM_000194	HPRT1	Hypoxanthine phosphoribosyltransferase 1
NM_001002	RPLP0	Ribosomal protein, large, P0

Table S4 Cell Surface Markers RT² Profiler PCR Array

Cells type	Surface markers gene list
B-Cell	
Activated B activated B cells	CD28, CD38, CD69, CD70, CD80, CD83, CD86, DPP4, FCER2, IL2RA (CD25), TNFRSF8
Mature B-cells	CD19, CD22, CD24, CD37, CD40 (TNFRSF5), CD72, CD74, CD79A, CD79B, CR2, IL1R2, ITGA2, ITGA3, MS4A1, ST6GAL1
Other B-cell	CD1C, CHST10, HLA-A, HLA-DRA, NT5E
T-cell	
Cytotoxic T-cells	CD8A, CD8B
Helper T-cells	CD4
Activated T-cells	ALCAM, CD2, CD38, CD40LG, CD69, CD70, CD83, CD96, CTLA4, DPP4, HLA-DRA, IL12RB1, IL2RA (CD25), ITGA1, TNFRSF4 (OX40), TNFRSF8
Other T-cell	CD160, CD247, CD28, CD37, CD3D, CD3G, CD5, CD6, CD7, FAS, KLRB1, KLRD1, NT5E, ST6GAL1
Natural killer (NK) cell	CD2, CD244, CD247, CD7, CD96, CHST10, IL12RB1, KLRB1, KLRC1, KLRD1, NCAM1
Monocyte & macrophage cell	
Activated macrophages	CD69, ENG (EVI-1), FCER2, IL2RA (CD25)
Other monocyte & macrophage cell	C5AR1 (GPR77), CD163, CD40 (TNFRSF5), CD63, CD70, CD74, CD86, CHST10, CSF1R, DPP4, FCGR1A, HLA-DRA, ICAM2, IL1R2, ITGA1, ITGA2, S100A8, TNFRSF8
Endothelial cell	ENG (EVI-1), ICAM2, NOS3 (eNOS), PECAM1, SELP, TEK (TIE-2, TIE2), VCAM1, VWF
Smooth muscle cell	MYH10, MYH9, MYOCD
Dendritic cell	CD1A, CD209, CD40 (TNFRSF5), CD83, CD86, CR2, FCER2
Mast cell	C5AR1 (GPR77), FCER1A, FCER2, TPSAB1
Fibroblast (stromal cell)	ALCAM, COL1A1, COL1A2
Epithelial cell	CD1D, EPCAM, KRT18, KRT5, KRT8
Adipocyte	RETN

Gene Description

GenBank	Symbol	Description
NM_001627	ALCAM	Activated leukocyte cell adhesion molecule
NM_001736	C5AR1	Complement component 5a receptor 1
NM_007053	CD160	CD160 molecule
NM_004244	CD163	CD163 molecule
NM_001770	CD19	CD19 molecule
NM_001763	CD1A	CD1a molecule
NM_001765	CD1C	CD1c molecule
NM_001766	CD1D	CD1d molecule
NM_001767	CD2	CD2 molecule
NM_021155	CD209	CD209 molecule
NM_001771	CD22	CD22 molecule
NM_013230	CD24	CD24 molecule
NM_016382	CD244	CD244 molecule, natural killer cell receptor 2B4
NM_000734	CD247	CD247 molecule
NM_006139	CD28	CD28 molecule
NM_001774	CD37	CD37 molecule
NM_001775	CD38	CD38 molecule
NM_000732	CD3D	CD3d molecule, delta (CD3-TCR complex)
NM_000073	CD3G	CD3g molecule, gamma (CD3-TCR complex)
NM_000616	CD4	CD4 molecule
NM_001250	CD40	CD40 molecule, TNF receptor superfamily member 5
NM_000074	CD40LG	CD40 ligand
NM_014207	CD5	CD5 molecule
NM_006725	CD6	CD6 molecule
NM_001780	CD63	CD63 molecule
NM_001781	CD69	CD69 molecule
NM_006137	CD7	CD7 molecule
NM_001252	CD70	CD70 molecule
NM_001782	CD72	CD72 molecule
NM_004355	CD74	CD74 molecule, major histocompatibility complex, class II invariant chain
NM_001783	CD79A	CD79a molecule, immunoglobulin-associated alpha
NM_000626	CD79B	CD79b molecule, immunoglobulin-associated beta
NM_005191	CD80	CD80 molecule
NM_004233	CD83	CD83 molecule
NM_006889	CD86	CD86 molecule
NM_001768	CD8A	CD8a molecule
NM_004931	CD8B	CD8b molecule
NM_005816	CD96	CD96 molecule
NM_004854	CHST10	Carbohydrate sulfotransferase 10
NM_000088	COL1A1	Collagen, type I, alpha 1
NM_000089	COL1A2	Collagen, type I, alpha 2
NM_001877	CR2	Complement component (3d/Epstein Barr virus) receptor 2
NM_005211	CSF1R	Colony stimulating factor 1 receptor
NM_005214	CTLA4	Cytotoxic T-lymphocyte-associated protein 4
NM_001935	DPP4	Dipeptidyl-peptidase 4
NM_000118	ENG	Endoglin
NM_002354	EPCAM	Epithelial cell adhesion molecule
NM_000043	FAS	Fas (TNF receptor superfamily, member 6)
NM_002001	FCER1A	Fc fragment of IgE, high affinity I, receptor for; alpha polypeptide
NM_002002	FCER2	Fc fragment of IgE, low affinity II, receptor for (CD23)
NM_000566	FCGR1A	Fc fragment of IgG, high affinity Ia, receptor (CD64)
NM_002116	HLA-A	Major histocompatibility complex, class I, A
NM_019111	HLA-DRA	Major histocompatibility complex, class II, DR alpha
NM_000873	ICAM2	Intercellular adhesion molecule 2
NM_005535	IL12RB1	Interleukin 12 receptor, beta 1
NM_004633	IL1R2	Interleukin 1 receptor, type II
NM_000417	IL2RA	Interleukin 2 receptor, alpha
NM_181501	ITGA1	Integrin, alpha 1
NM_002203	ITGA2	Integrin, alpha 2 (CD49B, alpha 2 subunit of VLA-2 receptor)
NM_002204	ITGA3	Integrin, alpha 3 (antigen CD49C, alpha 3 subunit of VLA-3 receptor)
NM_002258	KLRB1	Killer cell lectin-like receptor subfamily B, member 1
NM_002259	KLRC1	Killer cell lectin-like receptor subfamily C, member 1
NM_002262	KLRD1	Killer cell lectin-like receptor subfamily D, member 1
NM_000224	KRT18	Keratin 18
NM_000424	KRT5	Keratin 5
NM_002273	KRT8	Keratin 8
NM_021950	MS4A1	Membrane-spanning 4-domains, subfamily A, member 1
NM_005964	MYH10	Myosin, heavy chain 10, non-muscle
NM_002473	MYH9	Myosin, heavy chain 9, non-muscle
NM_153604	MYOCD	Myocardin
NM_000615	NCAM1	Neural cell adhesion molecule 1
NM_000603	NOS3	Nitric oxide synthase 3 (endothelial cell)
NM_002526	NT5E	5'-nucleotidase, ecto (CD73)
NM_000442	PECAM1	Platelet/endothelial cell adhesion molecule
NM_020415	RETN	Resistin
NM_002964	S100A8	S100 calcium binding protein A8
NM_003005	SELP	Selectin P (granule membrane protein 140 kDa, antigen CD62)
NM_003032	ST6GAL1	ST6 beta-galactosamide alpha-2,6-sialyltransferase 1
NM_000459	TEK	TEK tyrosine kinase, endothelial
NM_003327	TNFRSF4	Tumor necrosis factor receptor superfamily, member 4
NM_001243	TNFRSF8	Tumor necrosis factor receptor superfamily, member 8
NM_003294	TPSAB1	Tryptase alpha/beta 1
NM_001078	VCAM1	Vascular cell adhesion molecule 1
NM_000552	VWF	Von Willebrand factor
NM_001101	ACTB	Actin, beta
NM_004048	B2M	Beta-2-microglobulin
NM_002046	GAPDH	Glyceraldehyde-3-phosphate dehydrogenase
NM_000194	HPRT1	Hypoxanthine phosphoribosyltransferase 1
NM_001002	RPLP0	Ribosomal protein, large, P0

Table S5 Characteristics of patients with colorectal carcinoma

Characteristic		Number	%
Age (years)	<60	19	43.2
	≥60	25	56.8
Sex	Female	26	59.1
	Male	18	40.9
Tumor size	≤3	21	47.7
	>3	23	52.3
Lymph node metastasis	Yes	28	63.6
	No	16	36.4
Distant metastasis	Yes	3	6.8
	No	41	93.2
TNM stage	I	12	27.3
	II	21	47.7
	III	8	18.2
	IV	3	6.8

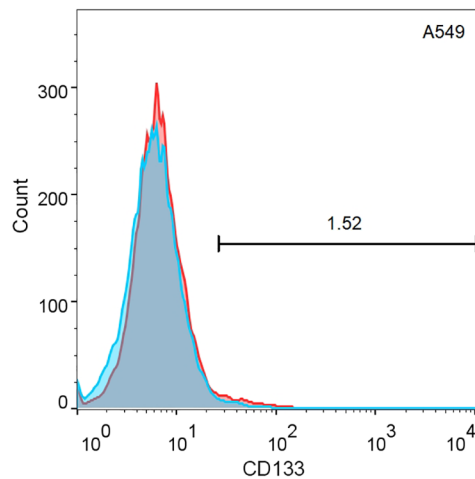


Figure S3 Representative expression of CD133⁺ cells in A549 detected by flow cytometry.

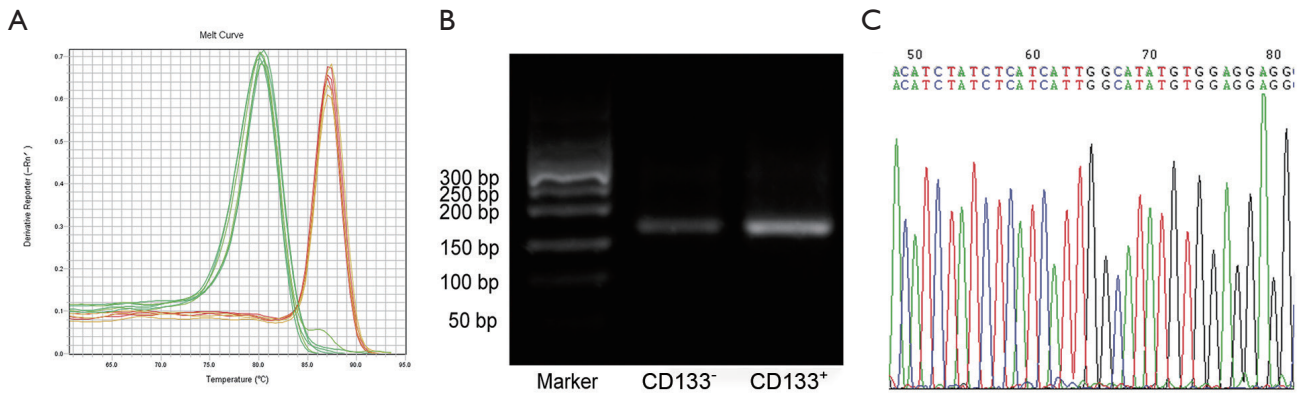


Figure S4 Verification of CD2. (A) Representative melting curves of CD2 in 2 clones. (B, C) Agarose gel analysis and representative Sanger sequencing result of real-time PCR amplified products (CD2). PCR, polymerase chain reaction.

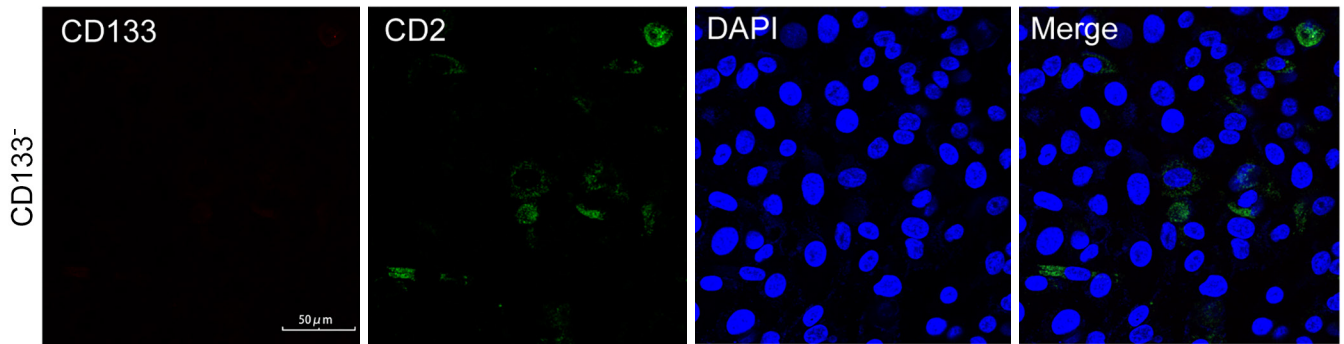


Figure S5 Immunofluorescence staining of CD2 (green) and CD133 (red) of CD133⁻ cells. Blue: nucleus. Scale bar: 50 μm.